

This is a repository copy of *A CLK1-KKT2 signaling pathway regulating kinetochore assembly in Trypanosoma brucei.*

White Rose Research Online URL for this paper:

<https://eprints.whiterose.ac.uk/173939/>

Version: Accepted Version

---

**Article:**

Saldivia, Manuel, Wollman, Adam J.M., Carnielli, Juliana B.T. et al. (5 more authors)  
(Accepted: 2021) A CLK1-KKT2 signaling pathway regulating kinetochore assembly in  
*Trypanosoma brucei*. MBio. ISSN 2150-7511 (In Press)

---

**Reuse**

Items deposited in White Rose Research Online are protected by copyright, with all rights reserved unless indicated otherwise. They may be downloaded and/or printed for private study, or other acts as permitted by national copyright laws. The publisher or other rights holders may allow further reproduction and re-use of the full text version. This is indicated by the licence information on the White Rose Research Online record for the item.

**Takedown**

If you consider content in White Rose Research Online to be in breach of UK law, please notify us by emailing [eprints@whiterose.ac.uk](mailto:eprints@whiterose.ac.uk) including the URL of the record and the reason for the withdrawal request.

**A CLK1-KKT2 signaling pathway regulating kinetochore assembly in *Trypanosoma brucei*.**

**Running title:** CLK1 regulates the trypanosome kinetochore

Manuel Saldivia<sup>a,b</sup>, Adam J. M. Wollman<sup>a,c</sup>, Juliana B.T. Carnielli<sup>a</sup>, Nathaniel G. Jones<sup>a</sup>, Mark C. Leake<sup>a,c</sup>, Christopher Bower-Lepts<sup>a</sup>, Srinivasa P.S. Rao<sup>b</sup> and Jeremy C. Mottram<sup>a#</sup>.

<sup>a</sup>York Biomedical Research Institute, Department of Biology, Heslington, University of York, YO10 5DD, UK,

<sup>b</sup>Novartis Institute for Tropical Diseases, 5959 Horton Street, Suite 900. Emeryville, CA 94608 USA

<sup>c</sup>York Biomedical Research Institute, Department of Physics, Heslington, University of York, YO10 5DD, UK.

# Corresponding author: [jeremy.mottram@york.ac.uk](mailto:jeremy.mottram@york.ac.uk)

**ABSTRACT**

During mitosis, eukaryotic cells must duplicate and separate their chromosomes in a precise and timely manner. The apparatus responsible for this is the kinetochore, which is a large protein structure that links chromosomal DNA and spindle microtubules to facilitate chromosome alignment and segregation. The proteins that comprise the kinetochore in the protozoan parasite *Trypanosoma brucei* are divergent from yeast and mammals and comprise an inner kinetochore complex comprising 24 distinct proteins (KKT1-23, KKT25) that include four protein kinases, CLK1 (KKT10), CLK2 (KKT19), KKT2 and KKT3. We recently reported the identification of a specific trypanocidal inhibitor of *T. brucei* CLK1, an amidobenzimidazole, AB1. We now show that chemical inhibition of CLK1 with AB1 impairs inner kinetochore recruitment and compromises cell cycle progression, leading to cell death. Here, we show that KKT2 is a substrate for CLK1 and identify phosphorylation of S508 by CLK1 to be essential for KKT2 function and for kinetochore assembly. Additionally, KKT2 protein kinase activity is required for parasite proliferation, but not for assembly of the inner kinetochore complex. We also show that inhibition or RNAi depletion of the Aurora kinase AUK1 does not affect CLK1 phosphorylation of KKT2, indicating that AUK1 and CLK1 are in separate regulatory pathways. We propose that CLK1 is part of a divergent signaling cascade that controls kinetochore function via phosphorylation of the inner kinetochore protein kinase KKT2.

38 **IMPORTANCE**

39 In eukaryotic cells kinetochores are large protein complexes that link chromosomes to  
40 dynamic microtubule tips, ensuring proper segregation and genomic stability during cell  
41 division. Several proteins tightly coordinate kinetochore functions, including the protein  
42 kinase Aurora Kinase B. The kinetochore has diverse evolutionary roots. For example,  
43 trypanosomatids, single cell parasitic protozoa that cause several neglected tropical  
44 diseases, possess a unique repertoire of kinetochore components whose regulation during  
45 cell cycle remains unclear. Here we shed light on trypanosomatid kinetochore biology, by  
46 showing that the protein kinase CLK1 coordinates the assembly of the inner kinetochore  
47 by phosphorylating one of its components, KKT2, allowing the timely spatial recruitment  
48 of the rest of the kinetochore proteins and posterior attachment to microtubules, in a  
49 process that is Aurora Kinase B independent.

50

51 Abstract word count: 225

52 Importance word count: 125

53 Text word count: 5001

54

## INTRODUCTION

At the onset of cell division, the accurate distribution of genomic material is crucial for cell survival and development (1). Central to this process are the kinetochores, a centromere macromolecular protein complex that drives chromosome segregation in eukaryotes by connecting chromosomes to microtubules (2). The kinetochore is a large, highly dynamic machine assembled from multiple pathways that are temporally controlled (3). Kinetochores gather on opposite sides of a centromere region of each chromosome where spindle microtubules attach (4). In general, the kinetochore can be thought of as a different set of proteins, assembled by timing blocks. The inner kinetochore, composed of proteins that bind to DNA or centromeric chromatin, is also known as the Constitutive Centromere-Associated Network (CCAN) in vertebrates and fungi (5). As a cell enters mitosis, outer kinetochore proteins are assembled on this platform of inner kinetochore proteins, forming the interaction surface for spindle microtubules, allowing chromosome movement (6). Several inner kinetochore components associate with kinetochores throughout the cell cycle, while other inner kinetochore proteins are recruited to the outer surface, specifically in mitosis (7). They provide a landing platform for the spindle assembly checkpoint (SAC) proteins, ensuring the fidelity of chromosome segregation (8).

From yeast to humans, the majority of the CCAN assembly can be subdivided into four discrete units, and their stability depends critically on reciprocal interactions (6). Furthermore, the recruitment of components of the CCAN in these species depends on a specialized centromeric histone H3 variant, the centromere protein A (CENP-A) (9). The fact that some subunits are missing in certain lineages (10), highlights that much remains to be understood about the structural and functional contributions of these four CCAN complexes at the kinetochore. Functional studies indicate that the CCAN plays an active role in the efficient incorporation of CENP-A into centromeric nucleosomes (11), where afterwards, it is required either for the assembly of further kinetochore components thus functioning as a scaffold (2) or the regulation of kinetochore–microtubule dynamics (12).

The emergence of eukaryotes from prokaryotic lineages has involved a significant rise in cellular complexity (13). Research on kinetochores has provided a picture of the essential organization of kinetochores across species. However, the functionality and dynamic organization of the layers that made the kinetochore in some early branch organisms, such as the kinetoplastids, remain unclear (14). This is the case of *Trypanosoma brucei*, the causative agent of Human African trypanosomiasis (HAT), whose kinetochore assembles from a repertoire of unique proteins very divergent from other organisms (15). To date, a trypanosomatid inner kinetochore which contains 24 unique proteins (KKT1-23 and KKT25) has been identified (15, 16). Within this group, two proteins with protein kinase domains (KKT2-3) are constitutively localized to centromeres throughout the cell cycle, most likely acting as functional orthologues of the eukaryotic CCAN proteins (15, 16). In addition, this parasite has a set of KKT-interacting proteins (KKIP1-12), which are related to outer kinetochore proteins Ndc80 and Nuf2 (17) and a cohort of proteins localized to the nucleus during interphase and to the spindle during mitosis (NuSAPs) involved in regulating spindle dynamics and chromosome segregation (18).

Apart from KKT2 and KKT3, the *T. brucei* kinetochore contains two other protein kinases, CLK1 (KKT10) and CLK2 (KKT19) (15, 19). Previous studies have shown that CLK1 is essential for survival in the bloodstream form of this parasite (20, 21). As part of a drug discovery campaign, we recently identified the amidobenzimidazole AB1 as a trypanocidal covalent inhibitor of *T. brucei* CLK1. Detailed mode of action and target validation studies indicates that CLK1 is the main target of AB, which binds specifically to C215 residue at the hinge domain (22). Treatment of the bloodstream form with AB1 caused nuclear enlargement during metaphase concomitant with a G2/M cell cycle arrest. Furthermore, we demonstrated that CLK1 inhibition impaired nuclear KKT2 distribution (22), suggesting that CLK1 has a role in kinetochore assembly or regulation. In the insect procyclic form KKT4 and KKT7 phosphorylation has been shown to depend on KKT10/19 and the localization of KKT10/19 is tightly controlled to regulate the metaphase to anaphase transition (19). Given the clinical importance of *T. brucei* bloodstream forms for drug intervention and the advantage of using a chemical tool to study the kinetochore regulation, here we demonstrate that CLK1 phosphorylates KKT2 at S508 during early metaphase, and its inhibition affects the posterior recruitment of inner kinetochore components affecting chromosome segregation, in a pathway that is independent to Aurora Kinase B.

## RESULTS

### CLK1 inhibitor AB1 disrupts kinetochore dynamics in bloodstream form *T. brucei*.

Given the importance of kinetochore movement during metaphase in eukaryotes (23), we assessed the impact of *T. brucei* CLK1 activity on kinetochore dynamics using AB1 as a chemical tool. The expression and localization of kinetochore proteins, labelled with mNeonGreen, were assessed by confocal microscopy in the bloodstream form of the parasite (Fig.1A). Similar to previous observations in procyclic form cells (15, 17), we observed different kinetochore timings and patterns of expression throughout the cell cycle. By using the kinetoplast (K) and nucleus (N) configuration to define each cell cycle stage (24), we observed that KKT2 and KKT3 are constitutively expressed until anaphase; KKT1 and KKIP1 gradually load from S phase onwards until the end of mitosis, whilst KKT4, KKT5 expression is restricted to metaphase. Furthermore, KKT9 and KKIP7 expression diminish during anaphase, suggesting both proteins may be acting as scaffolds for the recruitment of multiple other components. Treatment with 5x EC<sub>50</sub> of AB1 for 6 h caused dispersal, to varying degrees, for KKT1, KKT2, KKT5, KKT9, KKT13, KKT14 and KKT20 from the defined foci of the kinetochore within the nucleus, while KKT3, KKT7, KKT11, KKIP1 and KKIP7 remained in distinct foci (Fig. 1 B, C and Fig. S1 A). Automated foci detection using sub-pixel precise single particle localization combined with image segmentation (25) and intensity quantification (26) determined that there was a significant reduction in foci intensity for KKT1, KKT2, KKT4, KKT5 and KKT9, but not KKT3 (Fig. 1 D and Fig. S1B, C). No degradation of these proteins was observed after treatment (Fig S1 D). These results suggest that although KKT2 and KKT3 are centromere-anchored proteins (15), they respond differently to CLK1 inhibition and that TbCLK1 is a critical regulator of inner kinetochore component dynamics.

### CLK1 phosphorylates KKT2 at position S508.

KKT2 and KKT3 protein kinases are likely components of the trypanosome inner kinetochore with functional equivalence to the constitutive centromere-associated network (CCAN), a canonical component of the eukaryotic inner kinetochore (27). Defective KKT2 clustering was also observed after CLK1 RNAi (22). It has been reported that phosphorylation of kinetochore proteins has critical roles in kinetochore organization and interaction during mitosis in mammals and yeast (28). Indeed, cell cycle regulated changes in the phosphorylation of *T. brucei* kinetochore components have been reported recently, where the regulation is coordinated with phosphorylation of essential protein kinases including CLK1 (19).

We speculated that KKT2 provides a platform on which the kinetochore multi-protein complex assembles, and that phosphorylation orchestrates this process. To address whether KKT2 might be a CLK1 substrate, we first analyzed mobility shifts of phosphorylated forms of KKT2 and KKT3 using Phos-tag™ gel electrophoresis (29). A low-mobility, non-phosphorylated form of KKT2 was detected after treatment with AB1 or after CLK1 depletion by RNAi, whilst KKT3 remained unaffected (Fig. S2). Six phosphorylation sites have been identified in KKT2 (S<sup>5</sup>, S<sup>8</sup>, S<sup>25</sup>, S<sup>507</sup>, S<sup>508</sup>, S<sup>828</sup>) (30) and we tested if these are important for KKT2 function by generating a KKT2 RNAi line (Fig. S3) with a recoded HA-tagged version of KKT2 integrated into the tubulin locus. This constitutively expressed KKT2 (*KKT2<sup>R</sup>*) is not susceptible to RNAi-mediated degradation and *KKT2<sup>R</sup>* complements the loss of function of KKT2 48 h after RNAi induction (Fig. 2 A). Replacement of Ser for Ala in KKT2 at positions S<sup>5</sup>, S<sup>8</sup>, S<sup>25</sup> and S<sup>828</sup> resulted in complementation of KKT2 function when expressed in the RNAi line. In contrast, dual replacement of the KKT2 phosphorylation sites S<sup>507</sup> and S<sup>508</sup> with Ala (*KKT2<sup>S507A-S508A</sup>*) failed to complement depletion of the wild type KKT2 with respect to parasite growth (Fig. 2B) or cell cycle progression after 48 h induction (Fig. 2C). The efficacy of RNAi knockdown of the endogenous *KKT2* alleles was retained in these derivative cell lines (Fig. S3A,B,C) demonstrating that the complementation effects were imparted by the recoded alleles. *KKT2<sup>S507A-S508A</sup>* had good expression levels in the cell (Fig 2 B, lower panel), but was mislocalised (Fig. S3D), providing a possible explanation for the phenotype observed. These defects phenocopy the effect of AB1 and show the importance of the two phosphorylation sites for the function of KKT2. To assess whether protein kinase activity is essential for KKT2 function an active site mutant was generated in *KKT2<sup>R</sup>* (*KKT2<sup>K113A</sup>*). A significant loss of function was observed after 48 h induction, indicating protein kinase activity is essential for KKT2 function, but not for regulating cell cycle progression (Fig. 2B, C).

To address whether CLK1 phosphorylates KKT2 directly at S<sup>507-508</sup> residues, we expressed a recombinant peptide (aa 486 - 536) of KKT2 including mutations of S507 and S508 residues. We demonstrated that recombinant CLK1 could phosphorylate recombinant KKT2 *in vitro* at positions S507-508 (Fig. 2D). Given the conservation of KKT2 S<sup>508</sup> in kinetoplastids, we then raised a phospho-specific antibody against KKT2<sup>S508</sup> to follow KKT2 phosphorylation through the *T. brucei* cell cycle and after treatment with AB1. The antibody specifically recognizes phosphorylation of KKT2<sup>S508</sup>,

as phosphorylated KKT2<sup>S508</sup> was depleted following *KKT2* or *CLK1* RNAi (Fig. 2 E, upper panel), or after treatment with AB1 in a cell line where KKT2 was endogenously tagged with Ty and mNG (Fig. 2E, lower panel; both endogenous KKT2 and Ty-mNG KKT2 are detected). In addition, the KKT2 phosphoantibody detects phosphorylated KKT2 in all the recoded mutants, except the KKT2<sup>S507A-S508A</sup> double mutant (Fig. S3E). KKT2<sup>S508</sup> phosphorylation was found to increase in S-phase after hydroxyurea synchronization and progressively decrease towards G1-phase (Fig. 2F), in correlation with the recent demonstration of dynamic KKT2 S508 phosphorylation during the cell cycle (31). Together, these data show that KKT2 phosphorylation is downstream of CLK1 in a kinetochore-specific signaling cascade and occurs during early metaphase.

We next assessed whether KKT2 phosphorylation is required for recruitment of proteins to the trypanosome kinetochore. KKT1 and KKT9 recruitment were impaired in the KKT2<sup>R</sup>S<sup>507A-S508A</sup>::KKT2 induced cell line (Fig. 3A - C), but not the KKT2<sup>R</sup> K<sup>113A</sup> induced line (Fig. S4A) underlining the importance of KKT2 phosphorylation by CLK1 for kinetochore assembly. Individual expression of phospho-mimetics S<sup>507E</sup> and S<sup>508E</sup> impaired KKT1 and KKT9 recruitment, but also affected the timing of events during mitosis, with a notable defect in nuclear abscission (Fig. S4B).

### **CLK1 and AUK1 are not part of the same signaling pathway.**

Faithful chromosome segregation relies on the interaction between chromosomes and dynamic spindle microtubules (32). Furthermore, spindle elongation is important for correct segregation of chromosomes during anaphase (33). To further examine if CLK1 inhibition impairs microtubule spindle dynamics, we observed the expression of the mitotic spindle by staining the parasites with KMX-1 antibody and analyzing the microtubule-associated protein 103 kDa (MAP103) (Fig. S5) (34), this showed that treatment with AB1 does not affect microtubule spindle formation (Fig. 4 A). Considering that CLK1 inhibition during metaphase results in an arrest in late anaphase (19, 22), it is likely that the function of CLK1 during cytokinesis is related to either the control of kinetochore-spindle microtubule attachment errors, or its interactions with the chromosomal passenger complex (CPC). Of note, it has been reported that *T. brucei* aurora kinase B has an important role during metaphase-anaphase transition and the initiation of cytokinesis via regulation of the CPC (35–37) and nucleolar and other spindle-associated proteins (NuSAPs) (38).

In mammals, kinetochore assembly is enhanced by mitotic phosphorylation of the Dsn1 kinetochore protein by aurora kinase B, generating kinetochores capable of binding microtubules and promoting the interaction between outer and inner kinetochore proteins (39). In *T. brucei*, aurora kinase B (TbAUK1) plays a crucial role in spindle assembly, chromosome segregation and cytokinesis initiation (37). Therefore, we asked if CLK1 and AUK1 are part of the same signaling pathway. We showed that treatment with AB1 does not affect spindle formation (Fig. 4 A), in contrast to the inhibition of AUK1 (40). AUK1 is a key component of the trypanosome CPC (41). To understand if CPC dynamics are impaired by CLK1 inhibition, we followed the localization of CPC1 throughout the cell cycle before and after AB1 treatment and following AUK1 inhibition

by Hesperadin (42). After treatment with AB1, CPC1 showed a dispersed nuclear pattern that progressively disappeared after abscission of the nucleus (Fig. 4 B middle). This was different from AUK1 inhibition by Hesperadin, which prevented trans-localization of the CPC from the spindle midzone, impairing initiation of cytokinesis (Fig. 4 B right). Finally, we confirmed that AUK1 is not involved in kinetochore assembly since neither KKT2<sup>S508</sup> phosphorylation nor KKT2 localization was affected by AUK1 inhibition by Hesperadin (Fig. 4 C). In addition, a cohort of divergent spindle-associated proteins have been described that are required for correct chromosome segregation in *T. brucei* (18). Therefore, we analysed the subcellular localizations of NuSAP1 and NuSAP2 during the cell cycle after CLK1 inhibition. NuSAP2 expression in the central portion of the spindle after metaphase release was compromised by CLK1 inhibition, whilst NuSAP1 remained unaffected (Fig. 4 D). NuSAP2 is a divergent ASE1/PRC1/MAP65 homolog, a family of proteins that localizes to kinetochore fibres during mitosis, playing an essential role in promoting the G2/M transition (43). Considering that NuSAP2 and KKT2 co-localise during interphase and metaphase (18), it is likely that KKT2 regulation by CLK1 influences posterior spindle stability and cytokinesis.

## DISCUSSION

The inner kinetochore complex of *T. brucei* is unusual in that none of the 24 identified KKT proteins have any sequence identity with CENP proteins of the Constitutive Centromere-Associated Network (CCAN) in yeast or vertebrates (15, 16). Four of the KKTs contain protein kinase domains and here we provide the first evidence of a unique protein kinase signaling pathway that regulates inner kinetochore function in bloodstream form *T. brucei*. KKT2 is a multi-domain protein, constitutively associated with the centromere during the cell cycle, which contains an N-terminal protein kinase domain, a central domain with a unique zinc finger domain and a C-terminal divergent polo box domain (PDB) (15). The PBD and the central domain are sufficient for kinetochore localization (44), but it is not clear if KKT2 binds directly to DNA or forms a protein complex at nucleosomes with other KKT proteins. In this study, we show that whilst KKT2 protein kinase activity is required for growth and replication of bloodstream form trypanosomes (Fig. 2 B), the localization of KKT1 and KKT9 to the kinetochore remained unaffected by the loss of KKT2 protein kinase activity (Fig. S4A). These data suggest that KKT2 protein kinase activity is required for a function of the kinetochore that is independent from assembly of its inner complex.

We also show that phosphorylation of the kinetochore, and specifically KKT2, is crucial for kinetochore assembly in bloodstream form *T. brucei*. Depletion of the kinetochore protein kinase CLK1 (KKT10) by RNAi, or inhibition with the CLK1 inhibitor AB1 is lethal due to disruption of kinetochore assembly (22). Multiple phosphorylation sites have been identified in KKT2 and a number are cell cycle regulated, including S508 (31), suggesting a regulatory role. Whilst we cannot discount phosphorylation of S507 or other sites as a requirement for kinetochore assembly, we only identified S508 to be essential, indicating that the other known phosphorylation sites cannot compensate for loss of phosphorylation on S508. S508 is located between the Cys-rich central domain and the C-terminal domain and phosphorylation might contribute to association of KKT2



with chromatin via its DNA binding domain. Indeed, the finding that KKT2<sup>S507A-S508A</sup> is mislocalised supports this hypothesis and the fact that the mutant protein can localise to the kinetochore in the presence of wild type KKT2 suggests that KKT2 is an oligomer and that the WT protein can recruit and retain the mutant protein on the kinetochore. As KKT2 protein kinase activity is not required for assembly of the kinetochore, phosphorylation of S508 seems less likely to regulate the kinase activity of KKT2.

By using chemical and molecular approaches, we demonstrate that phosphorylation of KKT2 in the bloodstream form during metaphase allows the spatial recruitment of inner kinetochore components. We provide evidence that KKT2 is phosphorylated by CLK1, but we cannot formally rule out the possibility of an intermediate kinase being involved. Recently, a study showed that in the procyclic form CLK1 kinase activity is essential for metaphase to anaphase transition, although its expression was dispensable for the recruitment of kinetochore components (19). This difference may be due to cell cycle regulators having different functions in the two developmental stages of *T. brucei* (45, 46), or because there can be protein turnover differences between life cycle stages (47). Indeed, CLK1 protein expression relative to CLK2 appears higher the bloodstream trypanosome (22) than the procyclic form (19).

In *T. brucei* bloodstream forms, we show that KKT2 is a substrate for CLK1. In mammals CLK protein kinases are found in the cytoplasm and in the nucleus, where they regulate alternative splicing through phosphorylation of serine/arginine-rich domains on splicing factors (48), as occurs with human CLK1 in association with the serine-arginine protein kinase 1 (SRPK1) (49). Human CLKs also activate the abscission checkpoint in human cells by phosphorylating Aurora Kinase B, most likely acting as upstream regulators (50). The role of CLKs in regulating splicing is conserved across many organisms, including *Plasmodium falciparum*, where inhibition of PfCLK1-3 is lethal to the parasite by preventing the splicing of essential genes (51). In *T. brucei* most genes are constitutively transcribed as polycistronic mRNAs that are resolved through trans-splicing (52), but it remains unclear if CLK1 also has a role in that process. It has been proposed that the unique domains structure of *T. brucei* kinetochore proteins is consistent with the *T. brucei* kinetochore having a distinct evolutionary origin (15, 44) and the finding of a unique CLK1/KKT2-centred regulation for kinetochore assembly supports that hypothesis.

As with most signaling networks, phosphorylation plays an essential role in the regulation of kinetochore functions, and multiple kinases have been found to regulate kinetochores (53). Key examples are Aurora kinase B, MPS1, BUB1, PLK1, and CDK1 (53, 54). From yeast to humans, most of the functions of Aurora kinase B require its incorporation into the CPC (55), and its dynamic localisation during the cell cycle (54). As a regulator of the kinetochore-microtubule attachment during mitosis, Aurora Kinase B contributes decisively to two feedback mechanisms, the error correction (EC) and spindle assembly checkpoint (SAC) (56). Furthermore, it promotes the inner and outer kinetochore interactions through phosphorylation of Dsn1 (39, 57, 58), a subunit of the Mis12 inner kinetochore complex, essential for kinetochore assembly (59). The *T. brucei*

Aurora Kinase B orthologue, TbAUK1, has distinctive roles in metaphase-anaphase transition, ensuring a proper spindle assembly, chromosome segregation as well as cytokinesis (37, 40). Alongside the parasite CPC, TbAUK1 associates with chromosomes during G2/M phase, and with kinetochores in metaphase, and finally localizes in the spindle midzone in anaphase (41), suggesting a possible role coordinating kinetochore recruitment and attachment. However, the potential role of this kinase in promoting kinetochore assembly has not yet been established or well separated from its regulatory function on mitosis.

In the *T. brucei* procyclic form, two kinetochore proteins, KKT4 and KKIP4, localize to the spindle during mitosis (17, 60). Our results suggest that localization/expression of key outer kinetochore proteins remains unaffected after CLK1 inhibition, whereas KKT4, recently described as a microtubule tip-coupling protein (60), remains in anaphase, suggesting end-on interaction defects of microtubules with kinetochores. The role of Aurora kinase B in the interaction of the inner and outer kinetochore interaction in yeast resembles our findings of TbCLK1 functions in the recruitment of inner kinetochore during metaphase. Conversely, our results indicate that both pathways act independently in *T. brucei*, or at least not involving inner plate recruitment through KKT2 phosphorylation, the stability of KKT2 localisation further support this hypothesis. Interestingly, inhibition of CLK1 affects CPC localisation at metaphase, and NuSAP2 during anaphase. Understanding that centromeric localization of CPC is required to correct errors in attachment (61), and NuSAPs stabilizes kinetochore microtubule during metaphase (62), it will be possible that during anaphase onset, CLK1 and TbAUK1 coordinates different layers of regulation of kinetochore microtubule attachment and spindle stabilisation. The fact that CLK1 co-purifies with TbMlp2 and NuSAP1, provides further support for this (18). Interestingly, NuSAP1-4 partially co-localises with KKT2 (a CLK1 substrate) during the cell cycle, and knockdown of NuSAP1 destabilizes the expression of KKT1, but also triggers an unequal nuclear division without affecting spindle assembly (18), similar to our findings with KKT2 phosphomutants. Future experiments are required to determine whether the CLK1-KKT2 axis regulation of inner kinetochore assembly in *T. brucei*, also requires a specific set of NuSAPs proteins.

Altogether, we propose a model where CLK1 progressively phosphorylates KKT2 during S phase, allowing the timely spatial recruitment of the rest of the kinetochore proteins and posterior attachment to microtubules (Fig. 5). It is possible that KKT2 is phosphorylated by CLK1 prior to recruitment to the kinetochore, but evidence suggests this would occur during early S-phase (32). Inhibition of CLK1 activity with AB1 leads to impaired inner kinetochore assembly and irreversible arrest in M phase, suggesting that this defect cannot be repaired by the parasite's checkpoint control, implying a dual function of CLK1 at different points during chromosome segregation. Considering the conservation of CLK1 between *T. brucei*, *T. cruzi* and *L. mexicana* (22), the bioactivity of AB1 against the three trypanosomatids and the conservation of KKT2 S508 phosphorylation site in *Leishmania* and *T. cruzi*, it is quite likely that this signaling pathway is conserved across the trypanosomatids.

## MATERIALS AND METHODS

**Parasites.** All transgenic *T. b. brucei* parasites used in this study were derived from monomorphic *T. b. brucei* 2T1 bloodstream forms (63) and were cultured in HMI-11 [HMI-9 (GIBCO) containing 10% v/v foetal bovine serum (GIBCO), Pen/Strep solution (penicillin 20 U ml<sup>-1</sup>, streptomycin 20 mg ml<sup>-1</sup>)] at 37 °C/5% CO<sub>2</sub> in vented flasks. Selective antibiotics were used as follows: 5 µg ml<sup>-1</sup> blasticidin or hygromycin and 2.5 µg ml<sup>-1</sup> phleomycin or G418. RNAi was induced *in vitro* with tetracycline (Sigma Aldrich) in 70% ethanol at 1 µg ml<sup>-1</sup>. Endogenous Ty, mNeonGreen was performed using the pPOTv6 vector (64) The generation of inducible TbCLK1 and KKT2 RNAi was generated as previously described (20).

**Plasmids.** Recoded *KKT2* was synthesized by Dundee Cell Products. The recoded *KKT2* sequence (*KKT2*<sup>R</sup>) codes for the same amino acid sequence as *KKT2* but only shares 94.23% nucleotide identity. All segments of identity between *KKT2* and *KKT2*<sup>R</sup> are less than 20 base pairs long. *KKT2*<sup>R</sup> was inserted into the plasmid pGL2243 using *Xba*I and *Bam*HI restriction sites, generating pGL2492. This plasmid is designed to constitutively express *KKT2* from the tubulin locus, with the addition of a C-terminal 6x HA tag. To express catalytically inactive *KKT2* and phospho-mutants, the active site lysine (K<sup>113</sup>) and serine (S<sup>5</sup>, S<sup>8</sup>, S<sup>25</sup> S<sup>507-S508</sup> and S<sup>828</sup>) were changed to alanine by mutating pGL2492, carrying the coding sequence for *KKT2*, using site directed mutagenic PCR. A list of primers is provided in Supplementary Methods. To generate individual *KKT2* recoded mutants, correspondent *KKT2*<sup>R</sup> plasmids (above) were transfected into the *KKT2* RNAi cell line. Localization of endogenous *KKT1* and *KKT9* in *KKT2*<sup>R</sup> mutants were assessed by microscopy after transfection of the correspondent mNG-*KKT1* or mNG-*KKT9* pPOTv6 vector into each recoded cell line.

**Immunofluorescence and cell cycle analysis.** Cells treated for 6 hours with compounds or DMSO were centrifuged at 1400 g for 10 min before washing twice with TDB-glucose at room temperature. Suspensions were centrifuged at 1000 g for 5 min and pipetted into 6-well microscope slides and dried at RT. Cells were fixed with 25µl of 2% paraformaldehyde diluted in PBS and incubated at room temperature for 5 min. Cells were washed in PBS to remove paraformaldehyde prior to washing twice more with PBS and permeabilized with 0.05% NP40 for 10 min. Cells were washed twice in PBS and dried at RT. Mounting media with DAPI was added to each well with a coverslip. Slides were kept at 4 °C before viewing using a Zeiss LSM 880 with Airyscan on an Axio Observer.Z1 invert confocal microscope.

Ty-NuSAP1 and Ty-NuSAP2 were detected by indirect immunofluorescence by using a mouse Imprint ® Monoclonal Anti-Ty1 antibody (clone BB2). Briefly, cells were harvested by centrifugation at 1400 g for 10 min at room temperature, washed, and resuspended in TDB-glucose. 2x10<sup>5</sup> cells were dried on slides, fixed in 1% paraformaldehyde (PFA) for 1 hr, washed with PBS, blocked with 50% (v/v) foetal bovine serum for 30 min and then incubated with anti-TY (1:800) diluted in 0.5% blocking reagent for 1 hr. Alexa-Fluor® 488 (anti-mouse) was used as secondary

antibody (Invitrogen<sup>TM</sup>). Cells were DAPI stained and visualized using a Zeiss LSM 880 with Airyscan on an Axio Observer.Z1 invert confocal microscope.

To study the spindle formation, wild type bloodstream forms were treated or not for 6 h with AB1 (5x EC<sub>50</sub>) or CLK1 RNAi cells treated or not with tetracycline for 24 h. Parasites were harvested by centrifugation at 1,400g for 10 min and then washed twice with *Trypanosoma* dilution buffer (TDB)-glucose at room temperature. Samples were fixed for 10 min in 2% w/v formaldehyde in PBS, followed by 5 min incubation with 1M Tris pH 8.5 to quench the fixation. The fixed cells were washed with PBS, suspended in PBS, and adhered to SuperFrost Plus<sup>TM</sup> Adhesion slides for 15 min. Attached parasites were then permeabilized with methanol at -20°C for 15 min and rehydrated with PBS followed by incubation with blocking buffer (5% bovine serum albumin, 0.1% Triton X-100 in PBS) for 1 h at room temperature. Cells were immunostained at room temperature for 1 h with KMX-1 antibody to detect the mitotic spindle. After three washes (0.1% Triton X-100 in PBS), samples were incubated for one hour with an Alexa Fluor 488-conjugated goat anti-mouse IgG (used at 1:300) secondary antibody. Finally, after three more times washes, the slides were mounted in ProLong<sup>TM</sup> Diamond Antifade Mountant with DAPI and examined by fluorescence microscopy. For analysis, 2K1N and 2K2N populations (n=80) were considered, and statistical significance determined using the Holm-Sidak t- test, with alpha = 0.05.

For cell cycle analysis, bloodstream form *T. brucei* cell lines were incubated or not for 6 h with AB compounds at a final concentration of 5X the individual EC<sub>50</sub> value for each compound (averaged from viability assays). Control cultures were treated with 0.5µl DMSO. Cultures were pelleted and cells were collected and washed once in *Trypanosoma* dilution buffer (TDB) supplemented with 5 mM of EDTA and resuspended in 70% methanol. Cells were centrifuged at 1400 g for 10 min to remove methanol and washed once in TDB 1x with 5mM EDTA. Cells were resuspended in 1ml TDB 1x with 5mM EDTA, 10µg ml<sup>-1</sup> of propidium iodide and 10µl of RNase A. Cell suspensions in 1.5 ml tubes were wrapped in foil to avoid bleaching by light. Cells were incubated for 30 min at 37°C in the dark until FACS analysis. Cells were analyzed for FACS using a Beckman Coulter CyAn ADP flow cytometer (excitation; 535, emission; 617). Cell cycle phase distribution was determined by fluorescence.

Hydroxyurea-induced synchronization of cell lines was obtained by incubating parasites in exponential growth phase with 10 µM of Hydroxyurea (HU) (Sigma Aldrich) for 6 hr. Removal of HU from the culture medium was achieved by centrifuging cells at 1400 g for 10 min, washing twice with fresh (drug free) medium and resuspending cells in medium lacking HU. Subsequently, samples were collected each hour for posterior cell cycle analysis by propidium iodide staining.

**Protein analysis.** KKT2 and KKT3 phosphorylation profile were analyzed by using a SuperSep Phos-tag<sup>TM</sup> Precast Gel (29) according to the manufacturing protocol. Briefly, Ty-mNG KKT2 and Ty-mNG KKT3 were incubated with 5x AB1 EC<sub>50</sub> for 18 hr and collected for analysis by WB in an EDTA-free RIPA lysis buffer. In parallel, the expression of both proteins was also analyzed after 24 hr TbCLK1 RNAi. After

electrophoresis, the gel was washed 5 times with 10 mM EDTA transfer buffer to improve transference. Then, the membrane was transferred to a PVDF membrane using a 0.1% SDS Tris-Glycine transfer buffer at 90 mA overnight at 4 °C. The membrane was blocked for 1 hour with 10% BSA and KKT2 and KKT3 phosphorylation pattern was analyzed by using an anti-Ty1 antibody (see Supplementary Methods for details).

Anti-phospho KKT2 S<sup>508</sup> was raised against a synthetic phosphopeptide antigen C-GTRVGS(pS\*)LRPQRE-amide, where pS\* represent phosphoserine. The peptide was conjugated to keyhole limpet hemocyanin (KLH) and used to immunize rabbits. Phosphopeptide-reactive rabbit antiserum was first purified by protein A chromatography. Further purification was carried out using immunodepletion by non-phosphopeptide resin chromatography, after which the resulting eluate was chromatographed on a phosphopeptide resin. Anti-antigen antibodies were detected by indirect ELISA with unconjugated antigens passively coated on plates, probed with anti-IgG-HRP conjugate, and detected with ABTS substrate. Posterior antigen specificity was confirmed by western blot using KKT2 RNAi and endogenous tagged KKT2 cell lines. Custom antibody was produced by Thermo Fisher Scientific.

For Western blotting parasites were washed with trypanosome dilution buffer (TDB) supplemented with 20 mM of glucose. After centrifugation, the samples were resuspended in the RIPA buffer (New England Biolabs, #9806S)) supplemented with protease and phosphatase inhibitors obtained from Promega and Roche Life Science respectively. All samples were quantified by *Bradford protein* assay (Bio-Rad), 25 µg of protein was loaded, resolved in a 4-20% NuPAGE Bis-Tris gel (Invitrogen) in NuPAGE MOPS running buffer and transferred onto Hybond-C nitrocellulose membranes (GE Healthcare) at 350 mA for 2 h or, for high molecular weight proteins, overnight at 4 °C.

After transfer, membranes were washed once in 1x TBST (tris-buffered saline (TBS), 0.01% Tween-20 (Sigma Aldrich)) for 10 min then incubated for 1 hour in blocking solution (1x TBST, 5% BSA) or, if required, overnight at 4 °C. Next, the membrane was rinsed for 10 min in 1X TBST and placed in blocking buffer containing the required primary antisera for 1 hour at room temperature or overnight at 4 °C. The membrane was then washed 3 times with TBST and placed in blocking solution containing the appropriate fluorescent secondary antisera for 1 hr. A list of antibodies is provided in Supplementary Methods.

#### *General Statistics.*

All statistical analysis was performed using GraphPad Prism 8 (<http://www.graphpad.com/scientific-software/prism/>). The appropriate tests were conducted and are as detailed in the corresponding figure legends.

## Bibliography

1. A. J. Holland, D. W. Cleveland, Boveri revisited: chromosomal instability, aneuploidy and tumorigenesis. *Nat. Rev. Mol. Cell Biol.* **10**, 478–487 (2009).
2. I. M. Cheeseman, A. Desai, Molecular architecture of the kinetochore-microtubule interface. *Nat. Rev. Mol. Cell Biol.* **9**, 33–46 (2008).
3. M. Hara, T. Fukagawa, Dynamics of kinetochore structure and its regulations during mitotic progression. *Cell Mol. Life Sci.* (2020), doi:10.1007/s00018-020-03472-4.
4. L. J. Vos, J. K. Famulski, G. K. T. Chan, How to build a centromere: from centromeric and pericentromeric chromatin to kinetochore assembly. *Biochem Cell Biol.* **84**, 619–639 (2006).
5. T. Hori et al., CCAN makes multiple contacts with centromeric DNA to provide distinct pathways to the outer kinetochore. *Cell.* **135**, 1039–1052 (2008).
6. A. Musacchio, A. Desai, A molecular view of kinetochore assembly and function. *Biology (Basel)*. **6** (2017), doi:10.3390/biology6010005.
7. Y. Yamagishi, T. Sakuno, Y. Goto, Y. Watanabe, Kinetochore composition and its function: lessons from yeasts. *FEMS Microbiol. Rev.* **38**, 185–200 (2014).
8. A. Musacchio, E. D. Salmon, The spindle-assembly checkpoint in space and time. *Nat. Rev. Mol. Cell Biol.* **8**, 379–393 (2007).
9. W. C. Earnshaw, Discovering centromere proteins: from cold white hands to the A, B, C of CENPs. *Nat. Rev. Mol. Cell Biol.* **16**, 443–449 (2015).
10. I. A. Drinnenberg, S. Henikoff, H. S. Malik, Evolutionary turnover of kinetochore proteins: A ship of theseus? *Trends Cell Biol.* **26**, 498–510 (2016).
11. M. Okada, K. Okawa, T. Isobe, T. Fukagawa, CENP-H-containing complex facilitates centromere deposition of CENP-A in cooperation with FACT and CHD1. *Mol. Biol. Cell.* **20**, 3986–3995 (2009).
12. A. C. Amaro et al., Molecular control of kinetochore-microtubule dynamics and chromosome oscillations. *Nat. Cell Biol.* **12**, 319–329 (2010).
13. S. Westermann, A. Schleiffer, Family matters: structural and functional conservation of centromere-associated proteins from yeast to humans. *Trends Cell Biol.* **23**, 260–269 (2013).
14. T. Cavalier-Smith, Kingdoms Protozoa and Chromista and the eozoan root of the eukaryotic tree. *Biol. Lett.* **6**, 342–345 (2010).
15. B. Akiyoshi, K. Gull, Discovery of unconventional kinetochores in kinetoplastids. *Cell.* **156**, 1247–1258 (2014).
16. O. O. Nerusheva, P. Ludzia, B. Akiyoshi, Identification of four unconventional kinetoplastid kinetochore proteins KKT22-25 in *Trypanosoma brucei*. *Open Biol.* **9**, 190236 (2019).
17. S. D’Archivio, B. Wickstead, Trypanosome outer kinetochore proteins suggest conservation of chromosome segregation machinery across eukaryotes. *J. Cell Biol.* **216**, 379–391 (2017).
18. Q. Zhou et al., Faithful chromosome segregation in *Trypanosoma brucei* requires a cohort of divergent spindle-associated proteins with distinct functions. *Nucleic Acids Res.* **46**, 8216–8231 (2018).

- 529 19. M. Ishii, B. Akiyoshi, Characterization of unconventional kinetochore kinases  
530 KKT10/19 in *Trypanosoma brucei*. J. Cell Sci. (2020), doi:10.1242/jcs.240978.
- 531 20. N. G. Jones et al., Regulators of *Trypanosoma brucei* cell cycle progression and  
532 differentiation identified using a kinome-wide RNAi screen. PLoS Pathog. **10**,  
533 e1003886 (2014).
- 534 21. M. Nishino, J. W. Choy, N. N. Gushwa, J. A. Osés-Prieto, Hypothemycin, a fungal  
535 natural product, identifies therapeutic targets in *Trypanosoma brucei*. Elife (2013).
- 536 22. M. Saldivia et al., Targeting the trypanosome kinetochore with CLK1 protein  
537 kinase inhibitors. Nat. Microbiol. **5**, 1207–1216 (2020).
- 538 23. A. Grancell, P. K. Sorger, Chromosome movement: kinetochores motor along.  
539 Curr. Biol. **8**, R382–5 (1998).
- 540 24. T. N. Siegel, D. R. Hekstra, G. A. M. Cross, Analysis of the *Trypanosoma brucei*  
541 cell cycle by quantitative DAPI imaging. Mol. Biochem. Parasitol. **160**, 171–174  
542 (2008).
- 543 25. A. J. Wollman et al., Transcription factor clusters regulate genes in eukaryotic cells.  
544 Elife. **6** (2017), doi:10.7554/eLife.27451.
- 545 26. M. C. Leake et al., Stoichiometry and turnover in single, functioning membrane  
546 protein complexes. Nature. **443**, 355–358 (2006).
- 547 27. A. P. Senaratne, I. A. Drinnenberg, All that is old does not wither: Conservation of  
548 outer kinetochore proteins across all eukaryotes? J. Cell Biol. **216**, 291–293 (2017).
- 549 28. M. Hara, T. Fukagawa, Kinetochore assembly and disassembly during mitotic entry  
550 and exit. Curr. Opin. Cell Biol. **52**, 73–81 (2018).
- 551 29. E. Kinoshita, E. Kinoshita-Kikuta, T. Koike, Separation and detection of large  
552 phosphoproteins using Phos-tag SDS-PAGE. Nat. Protoc. **4**, 1513–1521 (2009).
- 553 30. I. R. E. Nett et al., The phosphoproteome of bloodstream form *Trypanosoma*  
554 *brucei*, causative agent of African sleeping sickness. Mol. Cell Proteomics. **8**,  
555 1527–1538 (2009).
- 556 31. C. Benz, M. D. Urbaniak, Organising the cell cycle in the absence of transcriptional  
557 control: Dynamic phosphorylation co-ordinates the *Trypanosoma brucei* cell cycle  
558 post-transcriptionally. PLoS Pathog. **15**, e1008129 (2019).
- 559 32. G. E. Thomas, M. R. Renjith, T. K. Manna, Kinetochore-microtubule interactions  
560 in chromosome segregation: lessons from yeast and mammalian cells. Biochem. J.  
561 **474**, 3559–3577 (2017).
- 562 33. F. Severin, A. A. Hyman, S. Piatti, Correct spindle elongation at the  
563 metaphase/anaphase transition is an APC-dependent event in budding yeast. J. Cell  
564 Biol. **155**, 711–718 (2001).
- 565 34. H. Hayashi, B. Akiyoshi, Degradation of cyclin B is critical for nuclear division in  
566 *Trypanosoma brucei*. Biol. Open. **7** (2018), doi:10.1242/bio.031609.
- 567 35. S. C. Sampath et al., The chromosomal passenger complex is required for  
568 chromatin-induced microtubule stabilization and spindle assembly. Cell. **118**, 187–  
569 202 (2004).
- 570 36. M. Murata-Hori, Y. Wang, The kinase activity of aurora B is required for  
571 kinetochore-microtubule interactions during mitosis. Curr. Biol. **12**, 894–899  
572 (2002).

- 573 37. Z. Li, T. Umeyama, C. C. Wang, The Aurora Kinase in *Trypanosoma brucei* plays  
574 distinctive roles in metaphase-anaphase transition and cytokinetic initiation. PLoS  
575 Pathog. **5**, e1000575 (2009).
- 576 38. T. Sardon et al., Uncovering new substrates for Aurora A kinase. EMBO Rep. **11**,  
577 977–984 (2010).
- 578 39. B. Akiyoshi, C. R. Nelson, S. Biggins, The aurora B kinase promotes inner and  
579 outer kinetochore interactions in budding yeast. Genetics. **194**, 785–789 (2013).
- 580 40. X. Tu, P. Kumar, Z. Li, C. C. Wang, An aurora kinase homologue is involved in  
581 regulating both mitosis and cytokinesis in *Trypanosoma brucei*. J. Biol. Chem. **281**,  
582 9677–9687 (2006).
- 583 41. Z. Li et al., Identification of a novel chromosomal passenger complex and its  
584 unique localization during cytokinesis in *Trypanosoma brucei*. PLoS One. **3**, e2354  
585 (2008).
- 586 42. N. Jetton et al., The cell cycle as a therapeutic target against *Trypanosoma brucei*:  
587 Hesperadin inhibits Aurora kinase-1 and blocks mitotic progression in bloodstream  
588 forms. Mol. Microbiol. **72**, 442–458 (2009).
- 589 43. A. P. Smertenko et al., Control of the AtMAP65-1 interaction with microtubules  
590 through the cell cycle. J. Cell Sci. **119**, 3227–3237 (2006).
- 591 44. O. O. Nerusheva, B. Akiyoshi, Divergent polo box domains underpin the unique  
592 kinetoplastid kinetochore. Open Biol. **6** (2016), doi:10.1098/rsob.150206.
- 593 45. X. Tu, C. C. Wang, The involvement of two cdc2-related kinases (CRKs) in  
594 *Trypanosoma brucei* cell cycle regulation and the distinctive stage-specific  
595 phenotypes caused by CRK3 depletion. J. Biol. Chem. **279**, 20519–20528 (2004).
- 596 46. T. C. Hammarton, J. Clark, F. Douglas, M. Boshart, J. C. Mottram, Stage-specific  
597 differences in cell cycle control in *Trypanosoma brucei* revealed by RNA  
598 interference of a mitotic cyclin. J. Biol. Chem. **278**, 22877–22886 (2003).
- 599 47. M. Tinti, M. L. S. Güther, T. W. M. Crozier, A. I. Lamond, M. A. J. Ferguson,  
600 Proteome turnover in the bloodstream and procyclic forms of *Trypanosoma brucei*  
601 measured by quantitative proteomics. [version 1; peer review: 3 approved].  
602 Wellcome Open Res. **4**, 152 (2019).
- 603 48. J. Prasad, J. L. Manley, Regulation and substrate specificity of the SR protein  
604 kinase Clk/Sty. Mol. Cell. Biol. **23**, 4139–4149 (2003).
- 605 49. B. E. Aubol et al., Release of SR Proteins from CLK1 by SRPK1: A symbiotic  
606 kinase system for phosphorylation control of Pre-mRNA splicing. Mol. Cell. **63**,  
607 218–228 (2016).
- 608 50. E. Petsalaki, G. Zachos, Clks 1, 2 and 4 prevent chromatin breakage by regulating  
609 the Aurora B-dependent abscission checkpoint. Nat. Commun. **7**, 11451 (2016).
- 610 51. M. M. Alam et al., Validation of the protein kinase PfCLK3 as a multistage cross-  
611 species malarial drug target. Science. **365** (2019), doi:10.1126/science.aau1682.
- 612 52. A. Günzl, The pre-mRNA splicing machinery of trypanosomes: complex or  
613 simplified? Eukaryotic Cell. **9**, 1159–1170 (2010).
- 614 53. A. T. Saurin, Kinase and Phosphatase Cross-Talk at the Kinetochore. Front. Cell  
615 Dev. Biol. **6**, 62 (2018).
- 616 54. H. Funabiki, D. J. Wynne, Making an effective switch at the kinetochore by  
617 phosphorylation and dephosphorylation. Chromosoma. **122**, 135–158 (2013).



55. R. R. Adams, M. Carmena, W. C. Earnshaw, Chromosomal passengers and the (aurora) ABCs of mitosis. *Trends Cell Biol.* **11**, 49–54 (2001).
56. C. Ditchfield et al., Aurora B couples chromosome alignment with anaphase by targeting BubR1, Mad2, and Cenp-E to kinetochores. *J. Cell Biol.* **161**, 267–280 (2003).
57. M. K. Bonner et al., Enrichment of Aurora B kinase at the inner kinetochore controls outer kinetochore assembly. *J. Cell Biol.* **218**, 3237–3257 (2019).
58. A. J. Broad, K. F. DeLuca, J. G. DeLuca, Aurora B kinase is recruited to multiple discrete kinetochore and centromere regions in human cells. *J. Cell Biol.* **219** (2020), doi:10.1083/jcb.201905144.
59. S. L. Kline, I. M. Cheeseman, T. Hori, T. Fukagawa, A. Desai, The human Mis12 complex is required for kinetochore assembly and proper chromosome segregation. *J. Cell Biol.* **173**, 9–17 (2006).
60. A. Llauro et al., The kinetoplastid kinetochore protein KKT4 is an unconventional microtubule tip-coupling protein. *J. Cell Biol.* **217**, 3886–3900 (2018).
61. J. Haase, M. K. Bonner, H. Halas, A. E. Kelly, Distinct roles of the chromosomal passenger complex in the detection of and response to errors in kinetochore-microtubule attachment. *Dev. Cell.* **42**, 640–654.e5 (2017).
62. C. Li et al., NuSAP modulates the dynamics of kinetochore microtubules by attenuating MCAK depolymerisation activity. *Sci. Rep.* **6**, 18773 (2016).
63. S. Alsford, T. Kawahara, L. Glover, D. Horn, Tagging a *T. brucei* RRNA locus improves stable transfection efficiency and circumvents inducible expression position effects. *Mol. Biochem. Parasitol.* **144**, 142–148 (2005).
64. S. Dean, J. D. Sunter, R. J. Wheeler, TrypTag.org: A trypanosome genome-wide protein localisation resource. *Trends Parasitol.* **33**, 80–82 (2017).

## Acknowledgments

This work was supported by the Wellcome Trust (069712). JCM is a Wellcome Trust Investigator (200807). We thank our colleagues in The Bioscience Technology Facility of University of York who provided insight and expertise that greatly assisted our microscopy and flow cytometry research. We thank Keith Gull for providing the KMX-1 antibody.

J.C.M and S.P.S.R designed research; M.S., C.B-L., J.B.T.C and N.G.J performed research. M.S, A.J.M.W and M.C.L. analyzed data; J.C.M, S.P.S.R, and M.S prepared and wrote the manuscript. All authors reviewed, edited and approved the paper.

## Figure legends

**Figure 1. CLK1 inhibition impairs inner kinetochore dynamics.** (A) Scheme of the kinetochore assessment workflow by immunofluorescence. A representative cohort of kinetochore components were endogenously labelled with mNeonGreen (mNG) in *T. brucei* bloodstream forms. Fixed parasites in metaphase or anaphase were considered for analysis of kinetochore pattern and intensity. (B) Localization of inner (top panel) and outer (lower panel) kinetochore core components after CLK1 inhibition by AB1. Parasites were incubated or not for 6 hr with 5x EC<sub>50</sub> AB1. Representative fluorescence microscopy micrographs, showing bloodstream form parasites endogenously expressing N-terminal mNeonGreen (mNG) tagged kinetochore proteins. Cells with 2K1N and 2K2N kinetoplast/nucleus configuration are shown. Cells were counterstained with DAPI to visualize DNA (cyan). The right panel shows the Nomarsky (DIC) corresponding images. Scale bar, 2µm. (C) Percentage of cells in metaphase (1N2K) and anaphase (2N2K) showing a defined kinetochore localization before and after AB1 treatment as in (a) (n>100 cells in each stage). (D) Intensity of KKT foci detected before (DMSO) and after AB1 treatment. The data represents 75% percentile of total foci intensity (n=80 kinetochores in each condition). Error bars, SEM; \*\* p<0.01, \*\*\*p < 0.001. ns not significant. (Mann–Whitney U test).

**Figure 2. CLK1 regulates KKT2 function by phosphorylation of S508.**

(A) Schematic representation showing known KKT2 phosphosites and phosphomutants. (B) *In vitro* growth profile of KKT2 RNAi, KKT2<sup>R</sup> and KKT2<sup>R</sup> phosphomutants and active site mutant. Bars showing cumulative fold over uninduced control counts over time following tetracycline induction of cell lines in culture. Error bars represent mean ± SEM of three replicates; P values were calculated using a Two-tailed Student's t-tests; where \*\* p<0.01, \*\*\*p < 0.001. Lower panel: Western blot of HA-KKT2 mutants. The expression of KKT2 phosphomutants mutants were detected using an anti-HA antibody. EF-1 alpha protein expression was used as the loading control. (C) Cell cycle profile of KKT2 RNAi, KKT2<sup>R</sup> and KKT2<sup>R</sup> phosphomutants. Bars showing G2/M ratio over uninduced control following tetracycline induction of cell lines in culture. Error bars represent SEM of 3 replicates. P values were calculated using a Two-tailed Student's t-tests; where \*\*\*p < 0.001. (D) Recombinant CLK1 (rCLK1) phosphorylates recombinant KKT2 *in vitro*. Recombinant fragment of KKT2 including S<sup>507-508</sup> (KKT2<sup>486-536</sup>) was used as substrate for rCLK1 by ADP-Glo™ Kinase Assay. The same fragment but including a S<sup>507A-S508A</sup> mutation (blue) was used as a control. Phosphorylation of maltose binding protein (MBP) and rCLK1 autophosphorylation (no substrate) was included as control. Error bars, SEM (n=3); \*\*\*p < 0.001 (Two-tailed Student's t-test). Conservation of amino acids surrounding KKT2 S507-508 in *T. brucei* (tb), *T. cruzi* (tc) and *L. mexicana* (lm) is shown to the right. (E) Specificity of KKT2 S<sup>508</sup> phospho-specific antibody. Top: CLK1 and KKT2 RNAi was induced in 2T1 parasites for 24 hr. KKT2 phosphorylation was analyzed by western blot using KKT2 S<sup>508</sup> phospho-specific antibody Bottom: Phosphorylation of KKT2 S<sup>508</sup> and Ty-mNG KKT2 S<sup>508</sup> after 18 hr treatment with 5x EC<sub>50</sub> AB1. EF-1 alpha protein expression was used as the loading control. (F) KKT2 S<sup>508</sup> phosphorylation during the cell cycle. Cells expressing Ty-mNG-tagged KKT2 were synchronized in late S phase by incubating with 10 µM hydroxyurea for 6 hr and released. After release, cells were collected after 0, 1, 2 or 3 hr and KKT2

S<sup>508</sup> phosphorylation was analyzed by western blot. Cell cycle progression was assessed by flow cytometry (left) by staining with propidium iodide. Data is representative of two biological replicates.

**Figure 3. Phosphorylation of KKT2 is required for kinetochore assembly.**

(A) Schematic representation showing the endogenous labelling of KKT1 or KKT9 in KKT2 recoded S507-508 phosphomutant. (B) Recruitment of KKT1 and KKT9 to the kinetochore is impaired in KKT2<sup>R</sup> S<sup>507-508A</sup> mutant. Representative fluorescence microscopy of BSF parasites endogenously expressing KKT1 or KKT9 tagged with mNeonGreen (mNG) at the N terminus. Cells were imaged 48 h after induction of the KKT2<sup>R</sup> S<sup>507-508A</sup> mutant. Cells were counter stained with DAPI to visualize DNA (cyan). Scale bar, 2µm. (C) Regulation of KKT1 and KKT9 in recoded KKT2 S507-508A parasites. Top: Expression of the recoded HA-KKT2 S507-508A mutant detected by Western blot using anti-HA antibody. EF-1 alpha protein expression was used as the loading control. Bottom: Intensity of mNG-KKT1 and mNG-KKT9 foci in recoded KKT2 S507-508A mutants. The data represents 75% percentile of total foci intensity (n>25 kinetochores in each condition). Error bars, SEM; \*\*\*p < 0.001 (Mann–Whitney U test).

**Figure 4. Localization of CPC1 after treatment with AB1 or Hesperadin.**

(A) Spindle formation after CLK1 inhibition or RNAi knockdown. Top panel: Parasites were left untreated or treated for 6 hr with 5x EC<sub>50</sub> AB1 and analyzed by confocal microscopy. Bottom panel: CLK1 was depleted by RNAi for 24 hr after addition of tetracycline and compared with the uninduced control. Cells with 2K1N and 2K2N kinetoplast/nucleus configuration were analysed and spindle formation was assessed by using mouse anti KMX-1 antibody. Graphic bars represent the percentage of cells with (grey) or without spindle (purple). Error bars, SEM (n>80 cells in each stage). ns not significant. (B) Ty-mNG-CPC1 expressing parasites were left untreated or treated for 6 hr with 5x EC<sub>50</sub> AB1 or 5x EC<sub>50</sub> Hesperadin and analyzed by confocal microscopy. Cells in metaphase and anaphase are shown. Cells were counterstained with DAPI to visualize DNA (cyan). The right panel shows the Nomarsky (DIC) corresponding images. (C) Inhibition of Aurora kinase (AUK1) does not affect KKT2 S<sup>508</sup> phosphorylation. Left: KKT2 S<sup>508</sup> phosphorylation analyzed by WB in parasites treated or not with 5x EC<sub>50</sub> and 2x EC<sub>50</sub> Hesperadin for 6 hr and 18 hr respectively. Concurrently, AB1 treatment was used as positive control in the same conditions. EF-1 alpha protein expression was used as the loading control. Right: Localization of TY-mNG KKT2 after 6 hr treatment with 5x EC<sub>50</sub> Hesperadin. Cells in metaphase are showed. Cells were counterstained with DAPI to visualize DNA (cyan). (D) Localization of Nucleolar and Spindle Associated Proteins. Representative fluorescence microscopy micrographs showing localization of Nucleolar and Spindle Associated Protein 1 (NuSAP1, top panel) and 2 (NuSAP2, lower panel), after CLK1 inhibition by AB1. Both proteins were endogenously tagged with a Ty at the N terminus. Cells with 2K1N and 2K2N configuration are shown. Cells were counterstained with DAPI to visualize DNA (cyan). Lower right panel shows the quantification in percentage of positive or negative expression of NuSAP2 (n=200) during anaphase in control (DMSO) or treated (AB1) parasites. Error bars, SEM; \*\*\*p < 0.001 Two-tailed Student's t-test. Scale bar, 2µm.

**Figure 5. Regulation of kinetochore assembly by CLK1.**

This schematic diagram summarizes the recruitment defects caused by inhibition of CLK1 by AB1. In untreated cells in metaphase (top panel), CLK1 phosphorylates KKT2, resulting in recruitment of inner kinetochore components, allowing posterior kinetochore assembly to outer kinetochore components. When CLK1 is inhibited by AB1 (lower panel, arrow head), phosphorylation of KKT2 S<sup>508</sup> is prevented, leading to a failure of recruitment of inner kinetochore components and consequent cell cycle arrest. We hypothesize that KKT2 binding to the centromere is compromised (KKT2?) after CLK1 inhibition (dashed circle). H3, histone H3

## Supplementary Material

### Figure S1. Inner kinetochore core components localization after CLK1 inhibition

(A) Localization of inner kinetochore core components KKT7, KKT11, KKT13, KKT14 and KKT20 after CLK1 inhibition by AB1. Representative fluorescence microscopy micrographs, showing bloodstream form parasites expressing N-terminal mNeonGreen (mNG) tagged KKTs. For KKT20, parasites express N-terminal mScarlet (mS) tagged protein. Cells with 2K1N and 2K2N kinetoplast/nucleus configuration are shown. Cells were counterstained with DAPI to visualize DNA (cyan). Scale bar, 2 $\mu$ m. (B) Graphic representation of strategy used for automated identification of kinetochore and background regions and quantification of fluorescence at kinetochore foci. The region of parasite body and nucleus is masked in white, and the region of interest (ROI) quantified for the kinetochore is highlighted with arrows. In this case, KKT2 foci detection in untreated cells was used as example. (C) The distribution of kinetochore foci, defined as fluorescence intensities, before and after treatment with AB1. Minima of 60 kinetochore foci were measured for each condition; individual points are shown as grey dots. Median (green) and interquartile ranges (IQR) are shown. \*\*  $p < 0.01$ , \*\*\* $p < 0.001$ . ns not significant. (Mann–Whitney U test). (D) Western blots comparing total protein levels of KKT proteins after 6 hr treatment with AB1 at 5x EC<sub>50</sub>. EF-1 $\alpha$  expression was used as the loading control.

### Figure S2. KKT2 phosphorylation is affected by AB1

KKT2 and KKT3 phosphorylation pattern after AB1 treatment or CLK1 depletion by RNAi. Phosphorylation pattern of endogenously tagged Ty-mNG KKT2 and Ty-mNG KKT3 cell lines treated or not with 5x EC<sub>50</sub> AB1 for 6 hr, or after 24 hr of CLK1 RNAi induction. Protein samples were collected and resolved using Phos-tag™ technologies.

**Figure S3:** Verification of endogenous *KKT2* RNAi penetrance throughout strain generation. (A) Schematic of strain derivatives for selected *KKT2* RNAi and recoded addback strains. (B) Schematic depicting key genetic features of endogenous *KKT2* and recoded *KKT2<sup>R</sup>* allowing specific RT-qPCR analysis of endogenous *KKT2* mRNA levels. (C) Results of relative quantitation of endogenous *KKT2* mRNA levels in denoted cell lines by RT-qPCR. Bars and error bars denote mean  $\pm$  range, n=4, values indicate p-value results of t-test comparing induced versus non-induced samples (D) Representative fluorescence microscopy micrographs showing partial mislocalization of recoded phosphomutant *KKT2<sup>S507-508A</sup>*, analyzed with anti-HA antibody. Cells with 2K1N and 2K2N kinetoplast/nucleus configuration are shown. Cells were counterstained with DAPI to visualize DNA (cyan). Scale bar, 2 $\mu$ m. (E) Residue specificity of *KKT2* phosphoantibody in recoded *KKT2* mutants. Note the absence of signal in the *KKT2<sup>S507-508A</sup>* mutant (arrow). Endogenous mutant expression was analyzed by using anti-HA antibody.

### Figure S4. KKT2 impact on KKT1 and KKT9 recruitment.

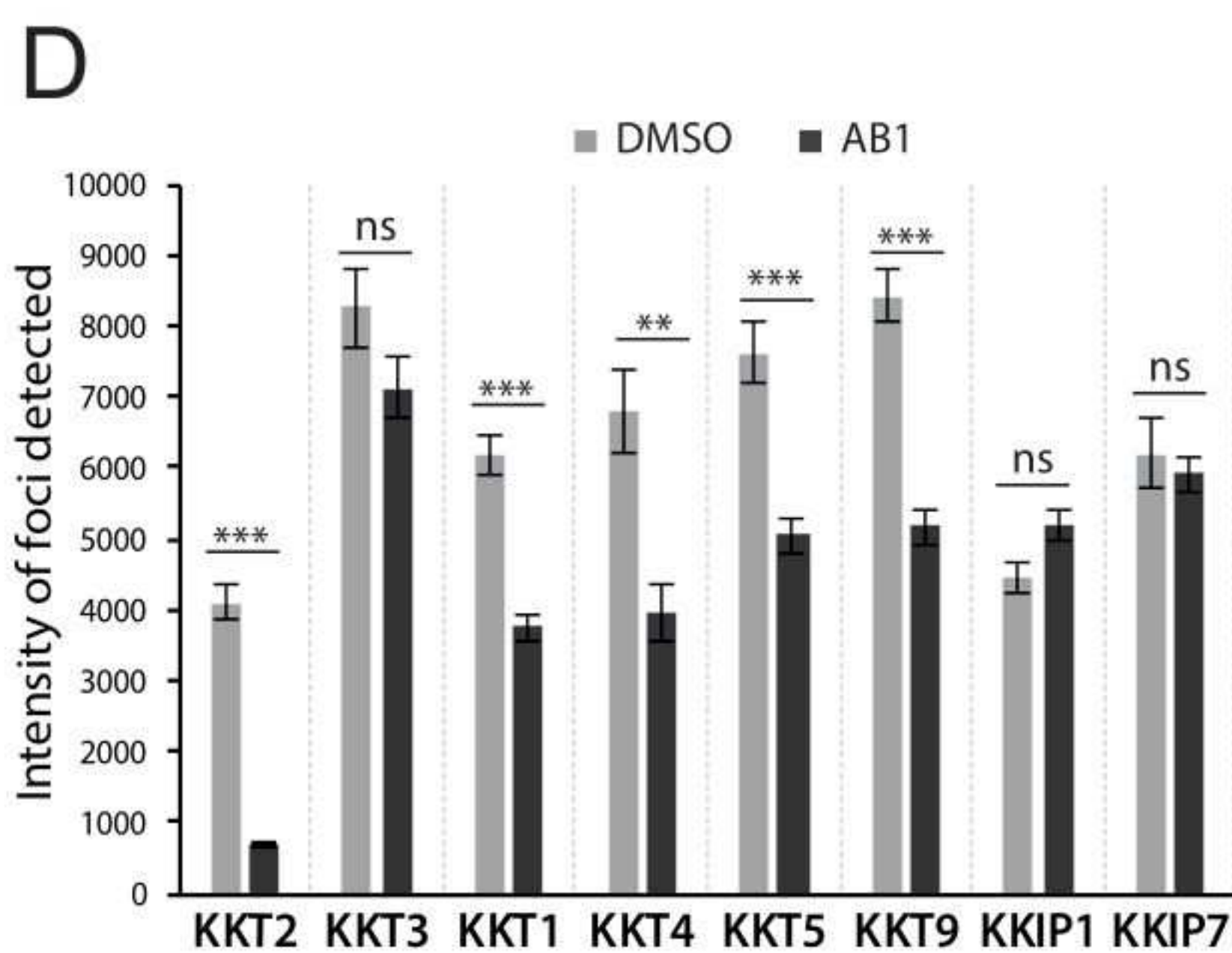
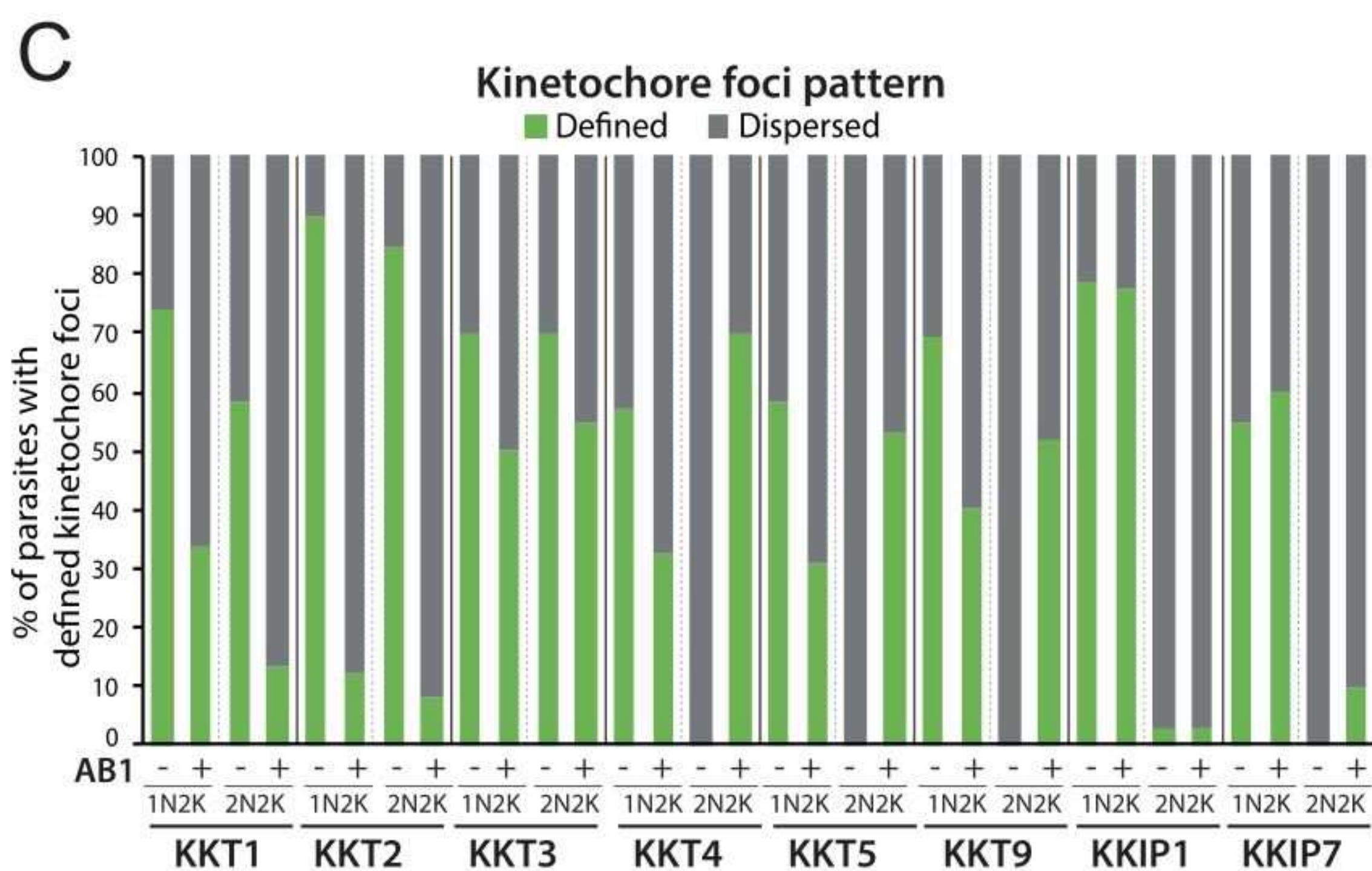
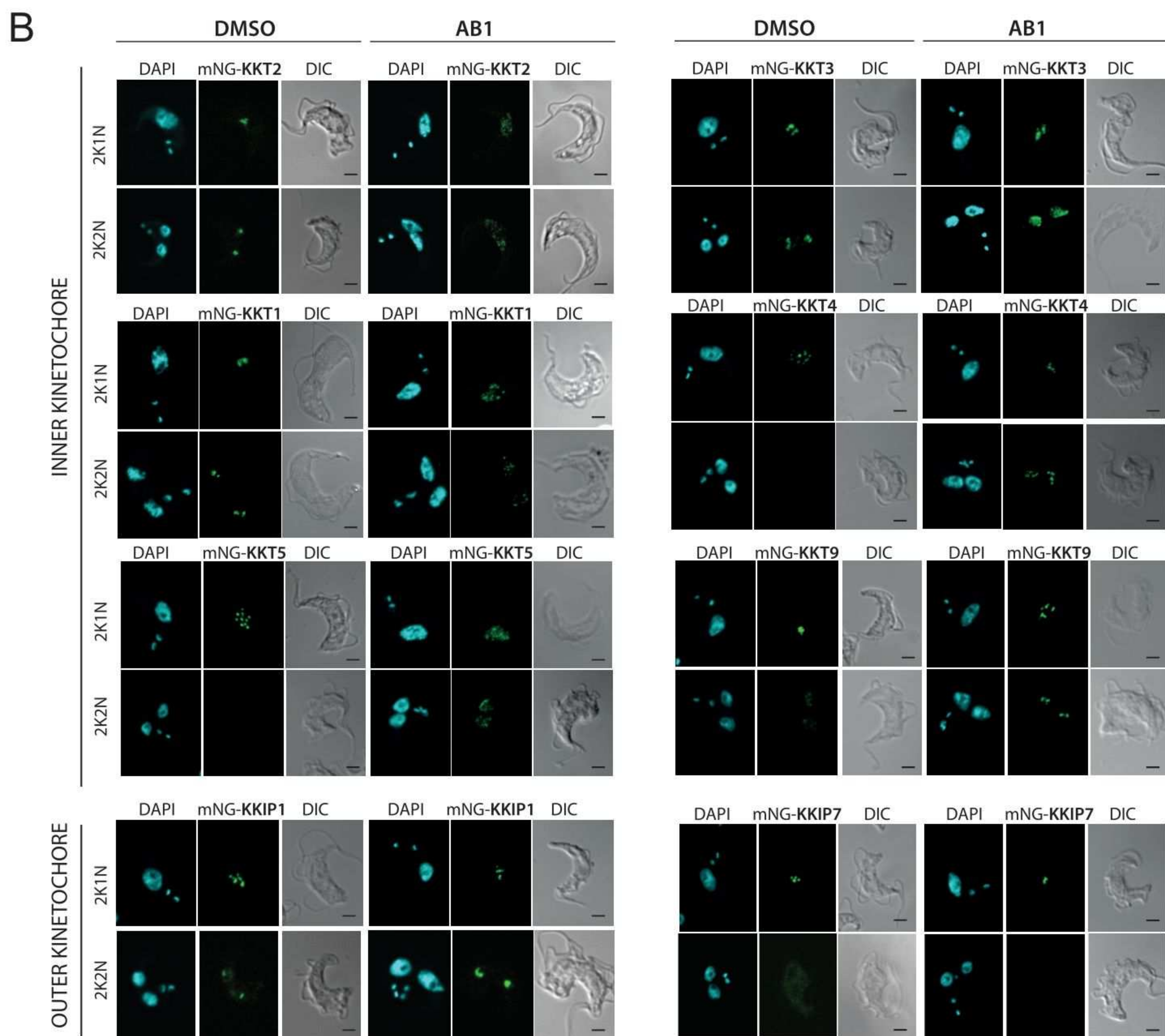
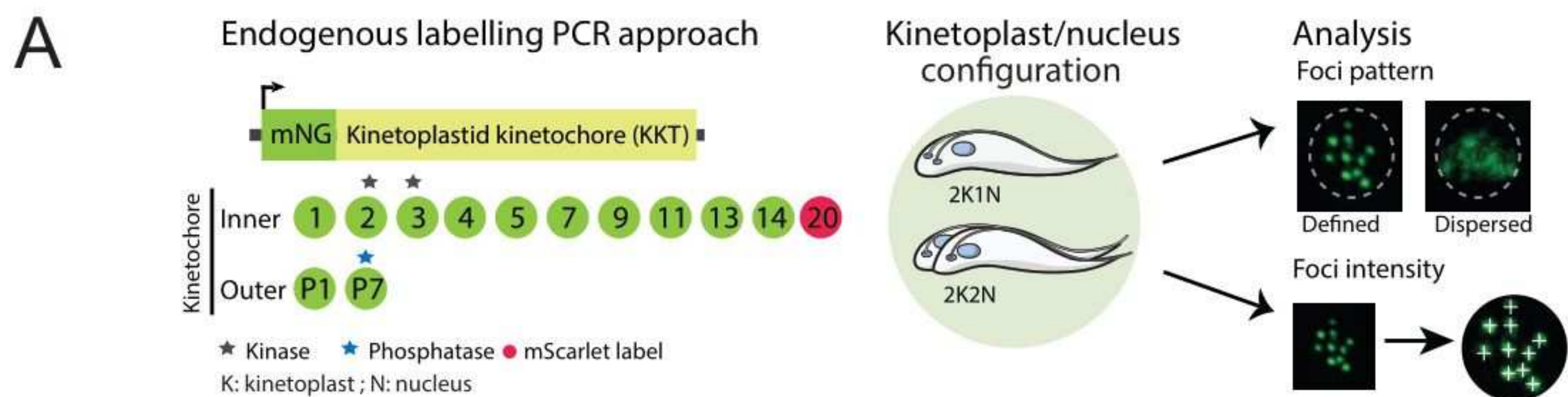
(A) Localization and expression pattern of inner kinetochore proteins KKT1 (left) and KKT9 (right) after expression of recoded catalytically inactive KKT2 R K<sup>113A</sup>. In both mutants, KKT1 and KKT9 proteins were tagged with mNeonGreen (mNG) at the N terminus. Cells with 2K1N and 2K2N kinetoplast/nucleus configuration are shown. Cells were counterstained with DAPI to visualize DNA (cyan). The right panel shows the Nomarsky (DIC) corresponding images. (B) Representative fluorescence microscopy micrographs showing localization of inner kinetochore proteins KKT1 (top panel) and KKT9 (bottom panel) after expression of recoded phosphomimetic KKT2R S<sup>507E</sup> (left panel) and KKT2R S<sup>508E</sup> (right panel). In both mutants, KKT1 and KKT9 proteins were tagged with mNeonGreen (mNG) at the N terminus. Abnormal nuclear shape after induction is shown with white arrows. Cells in metaphase and anaphase are shown. Cells were counterstained with DAPI to visualize DNA (cyan). The right panel shows the Nomarsky (DIC) corresponding images. Scale bar, 2μm.

**Figure S5. MAP103 expression after CLK1 inhibition by AB1**

Spindle formation after CLK1 inhibition. Parasites expressing mNG-MAP103 were left untreated or treated for 6 hr with 5x AB1 and analyzed by confocal microscopy. Error bars, SEM (n>100 cells in metaphase). ns not significant. lower: representative micrograph of each condition

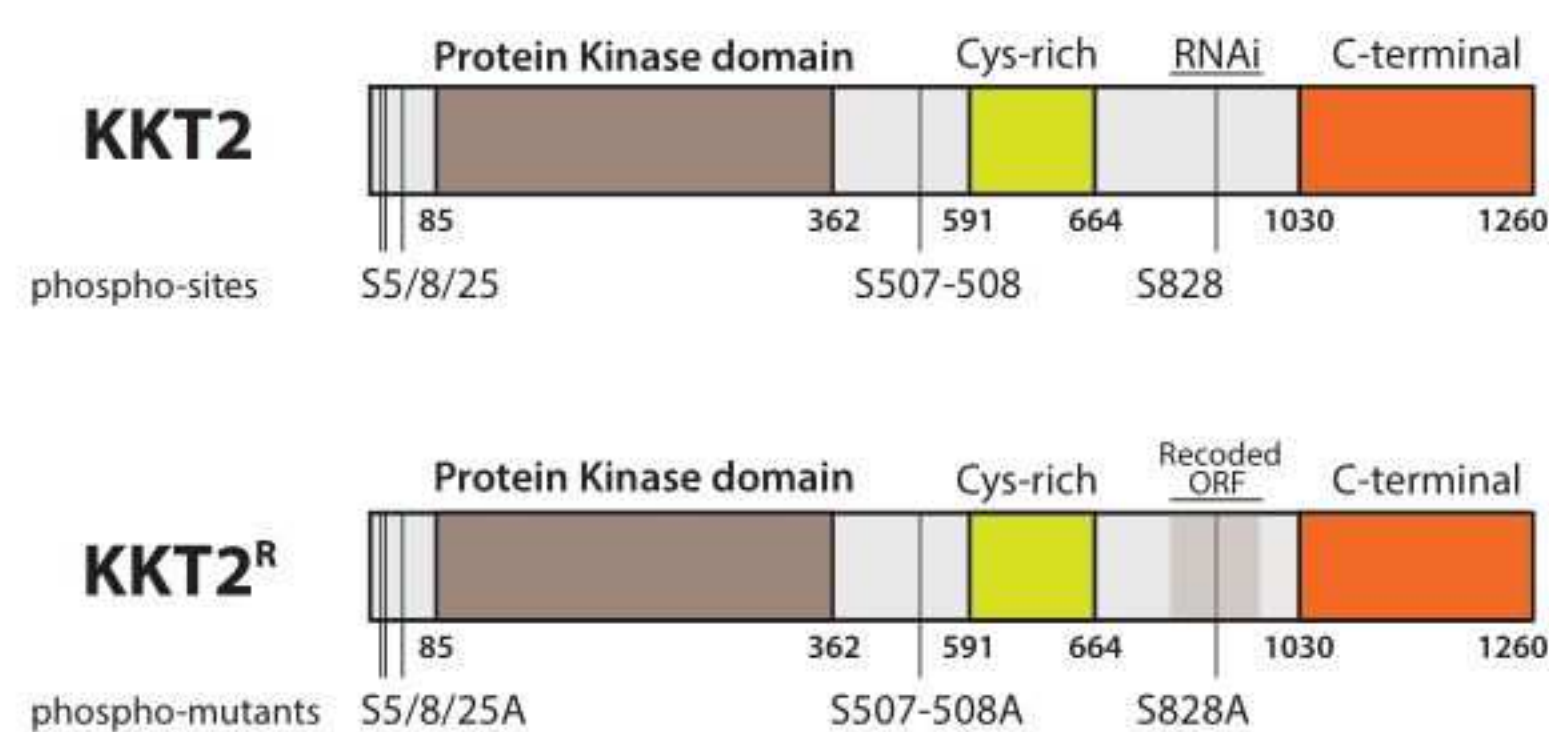
**Supplementary methods.** Additional methods not included in the main manuscript.



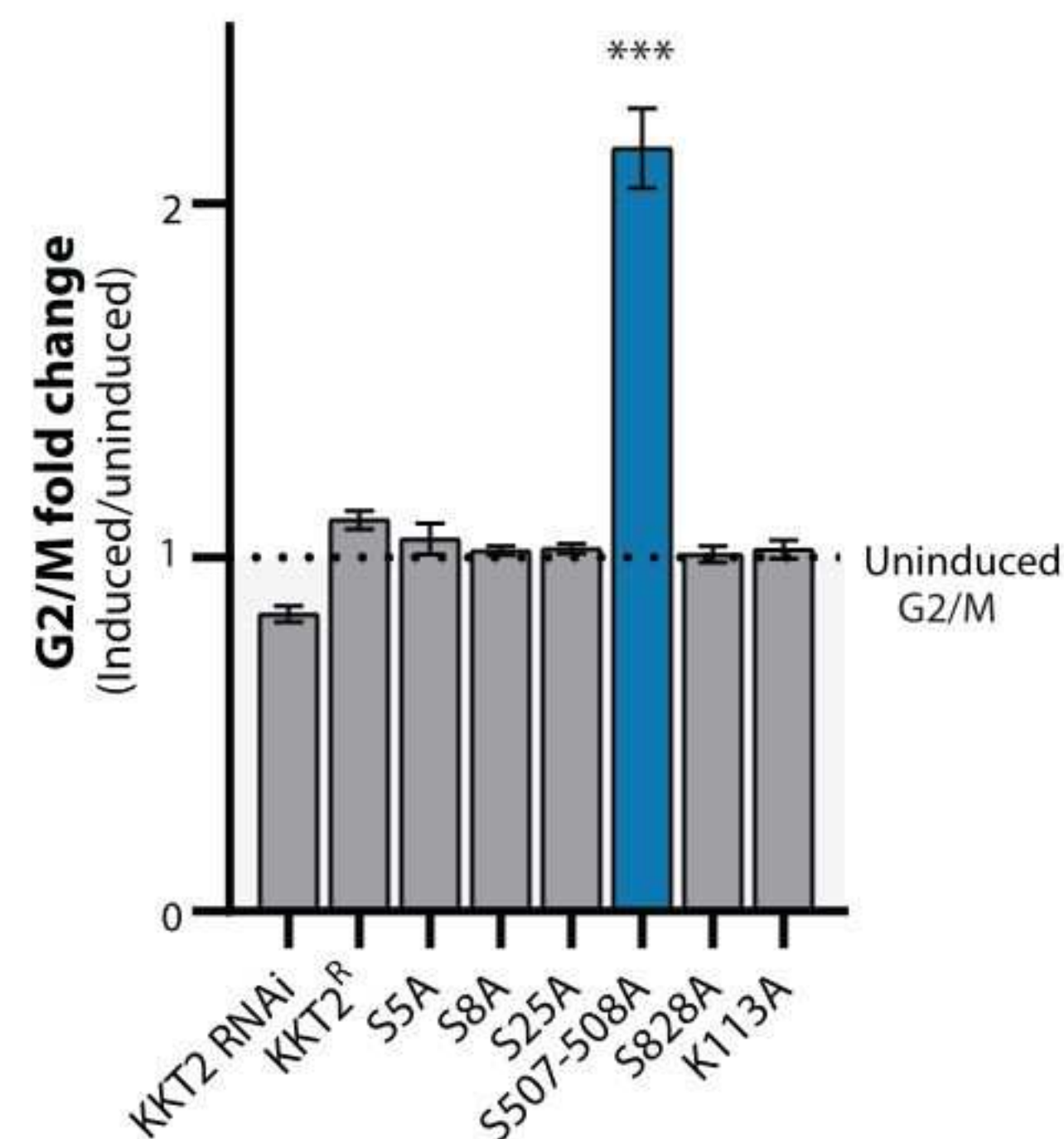




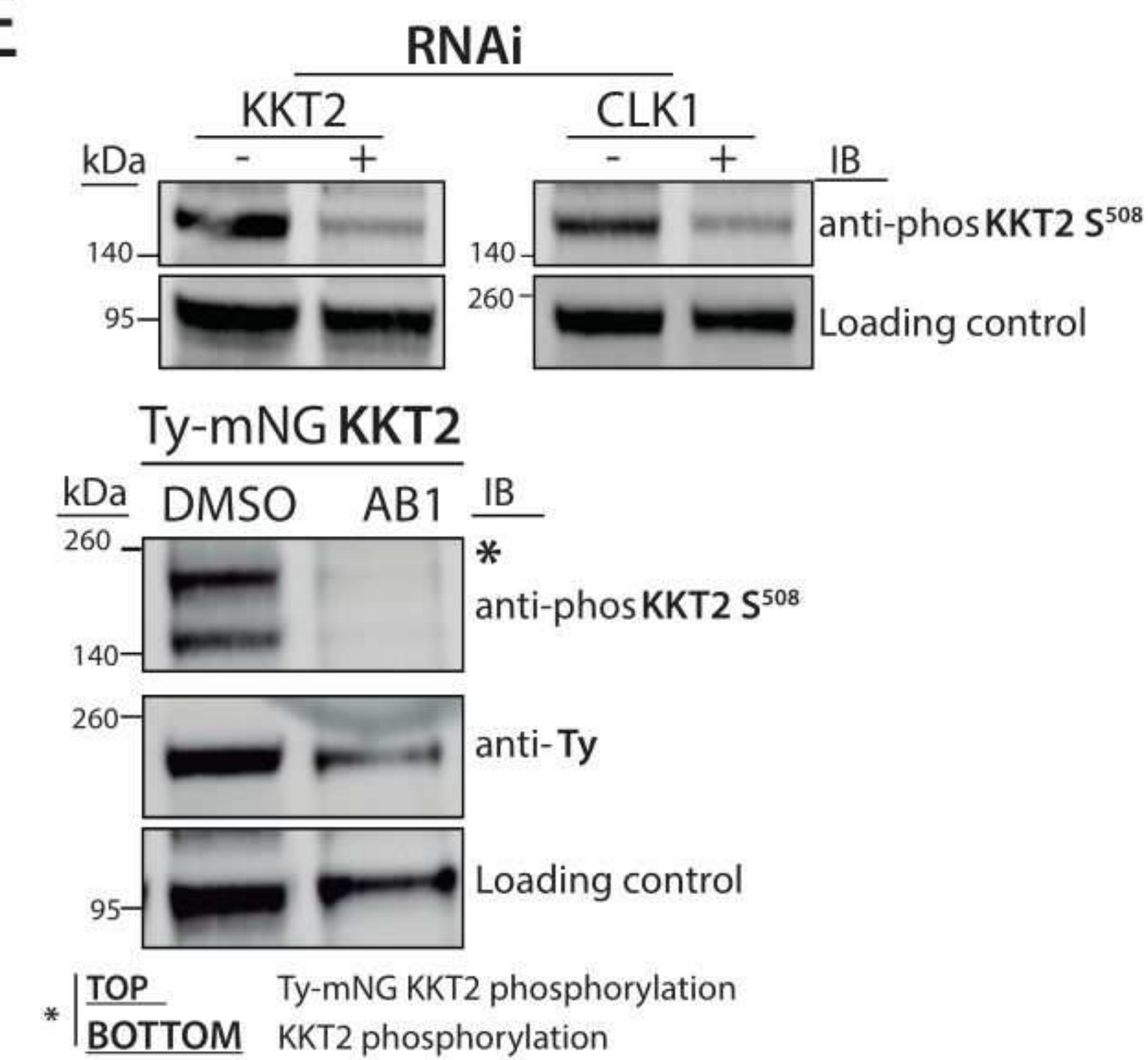
A



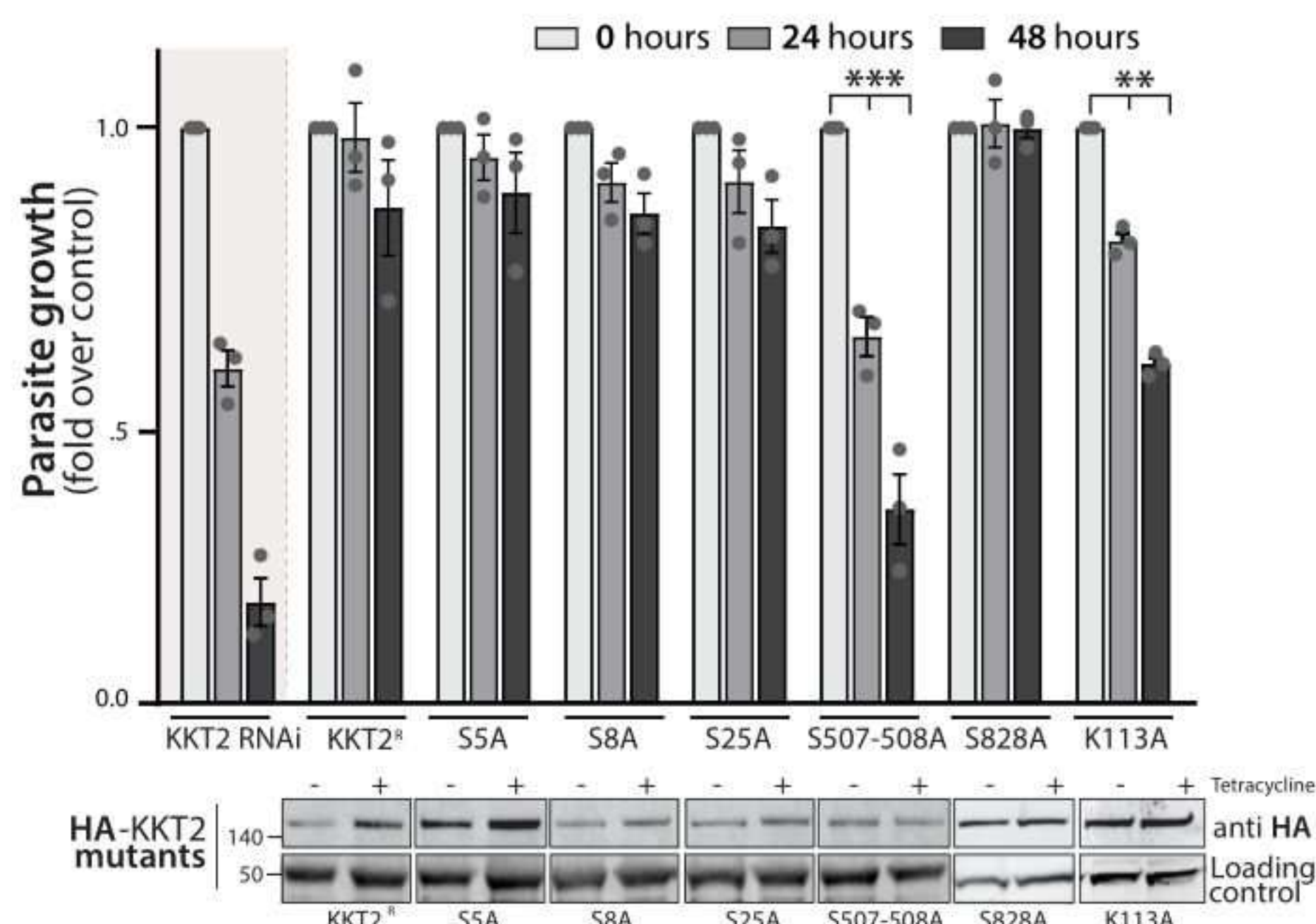
C



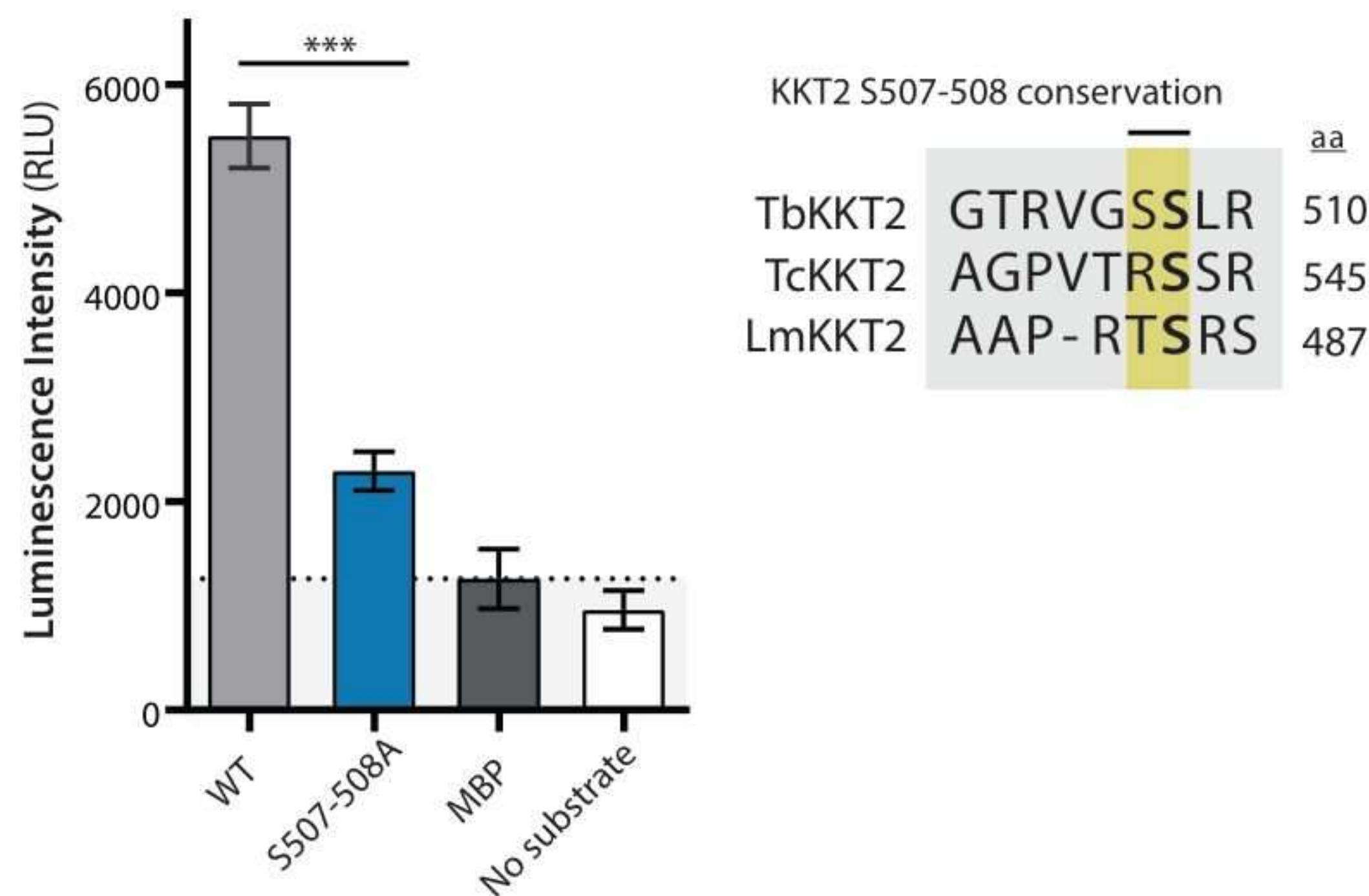
E



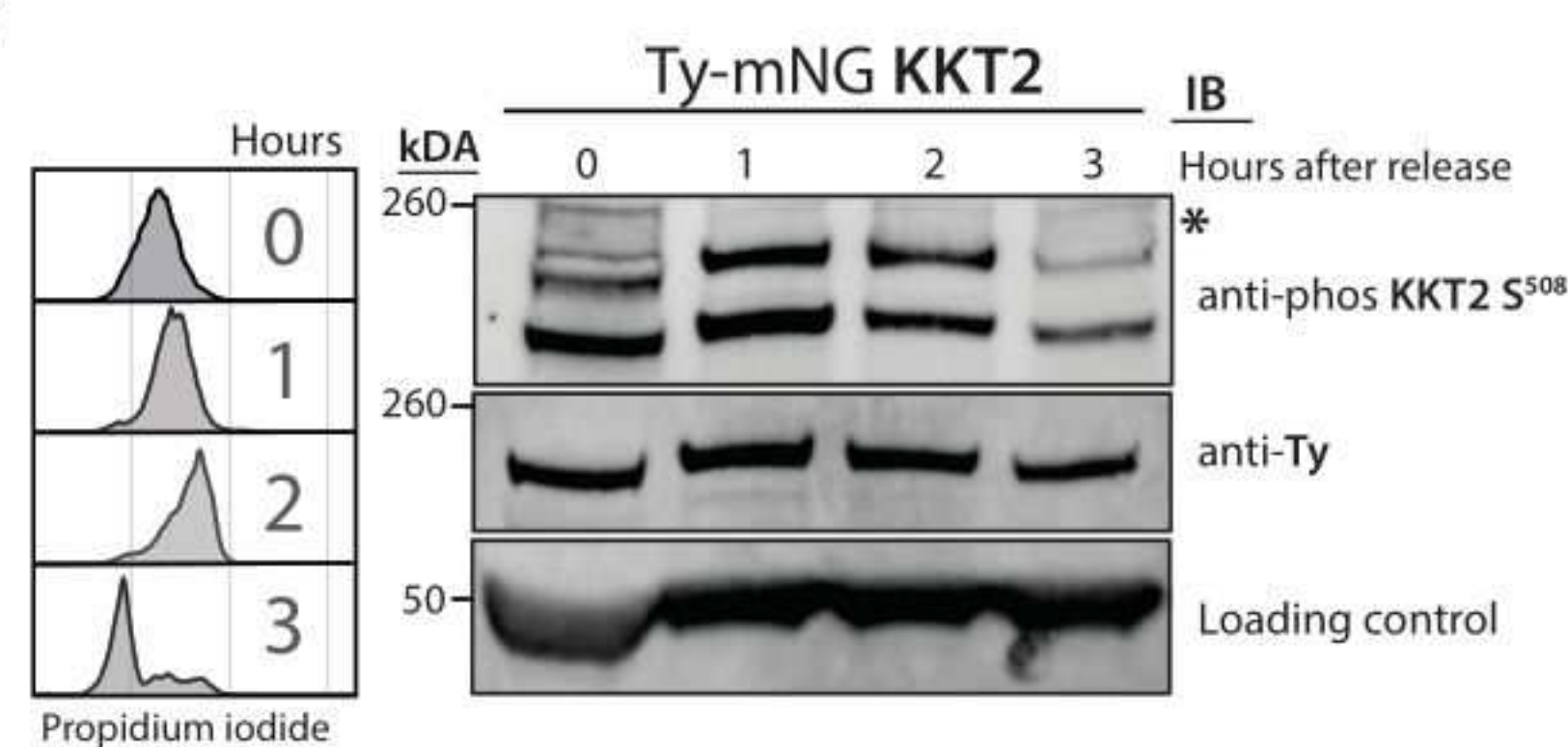
B



D

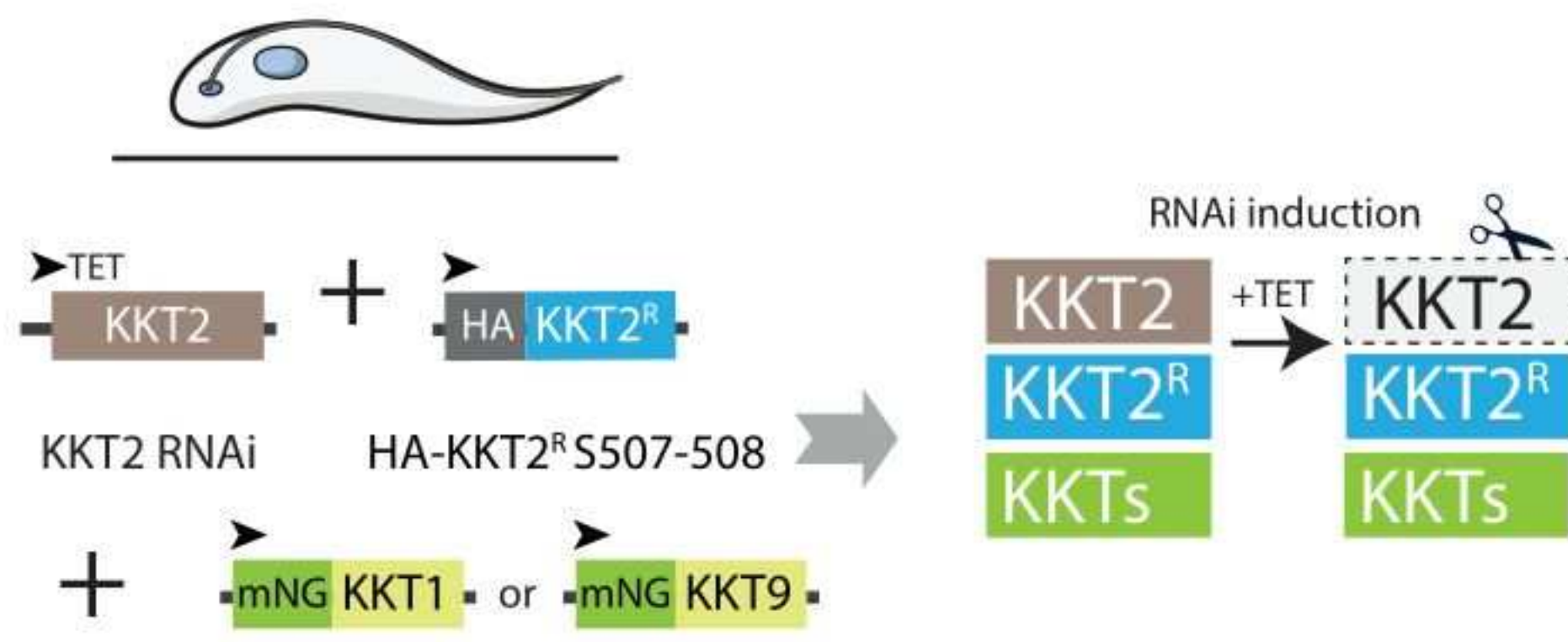


F

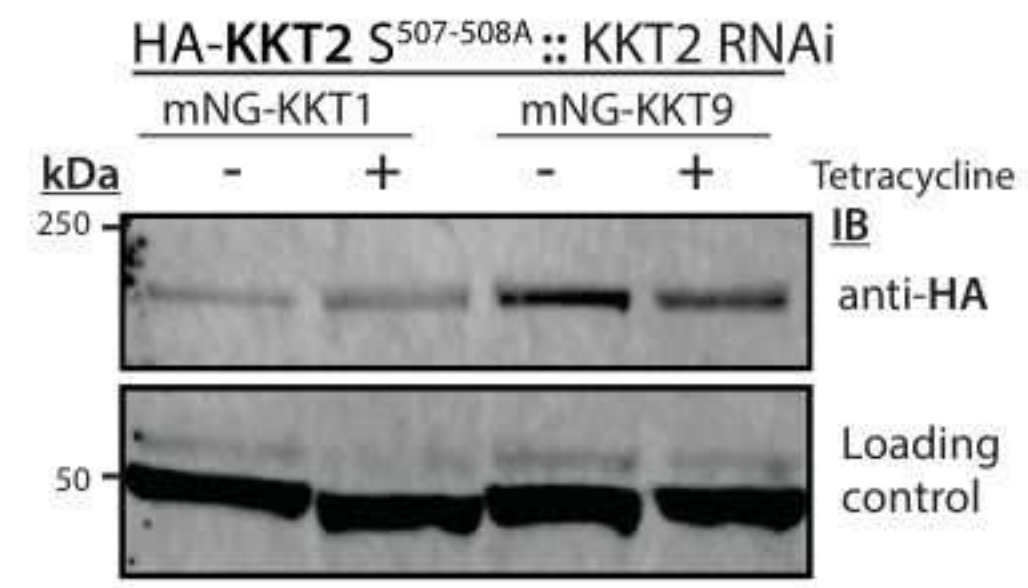




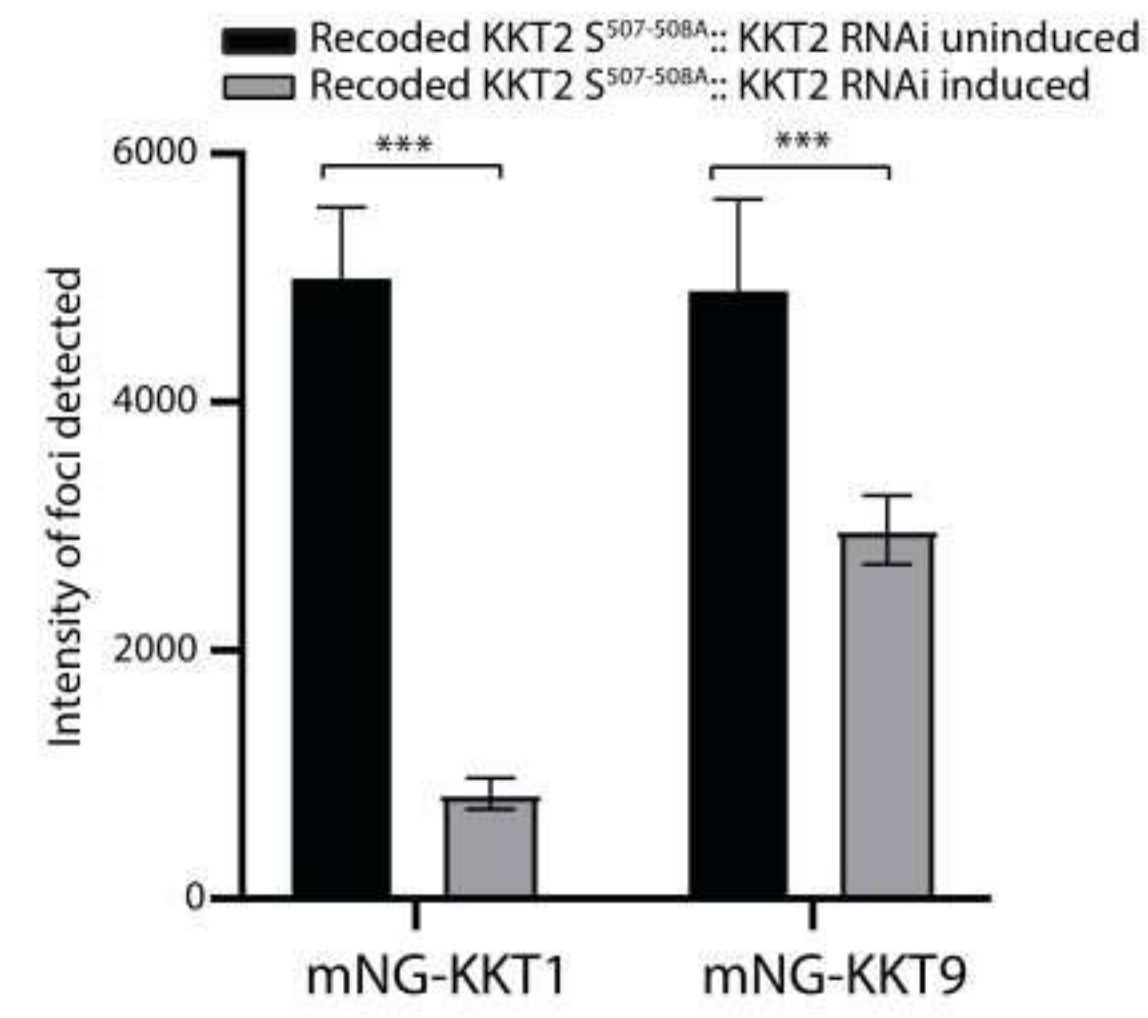
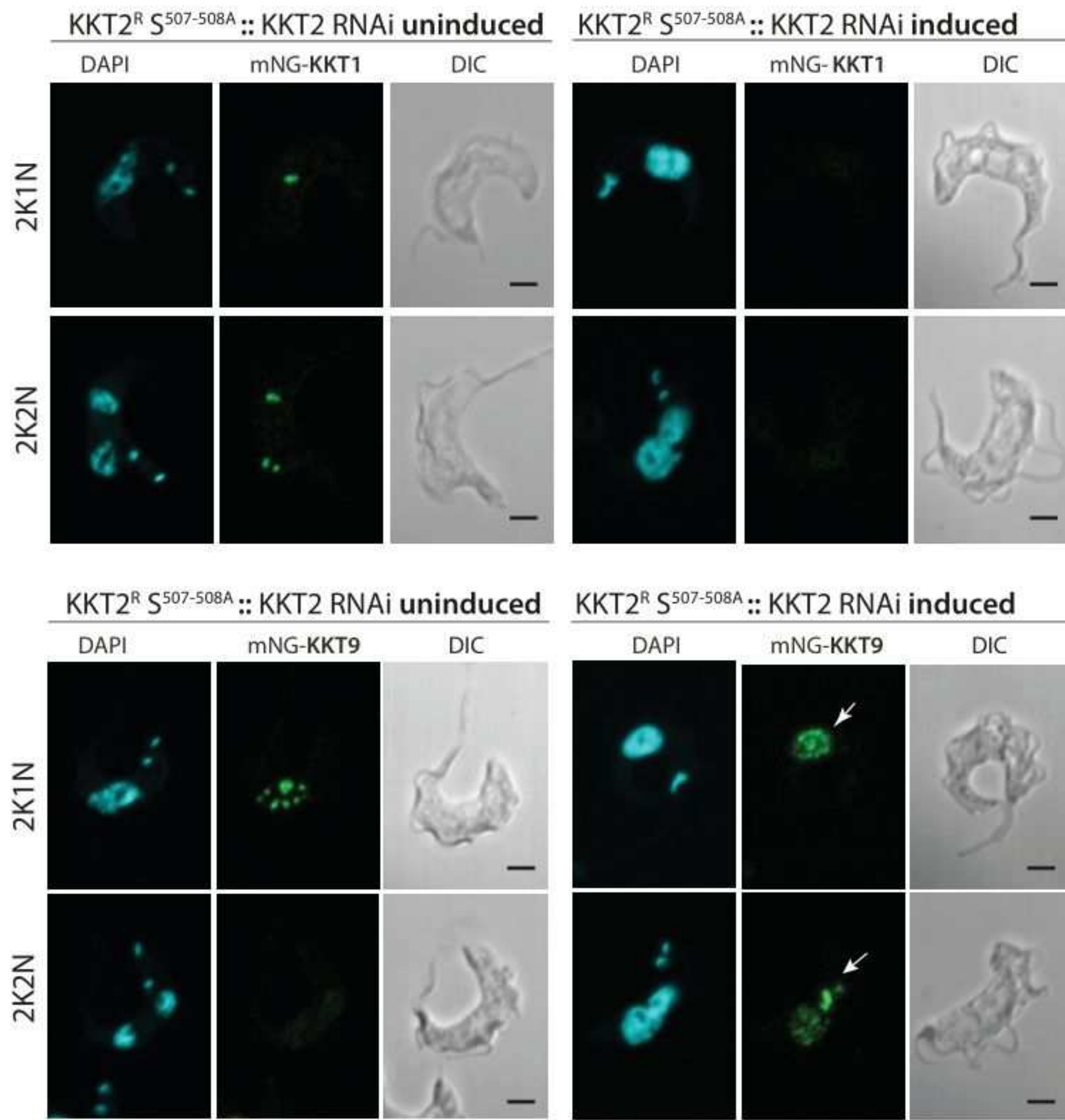
A



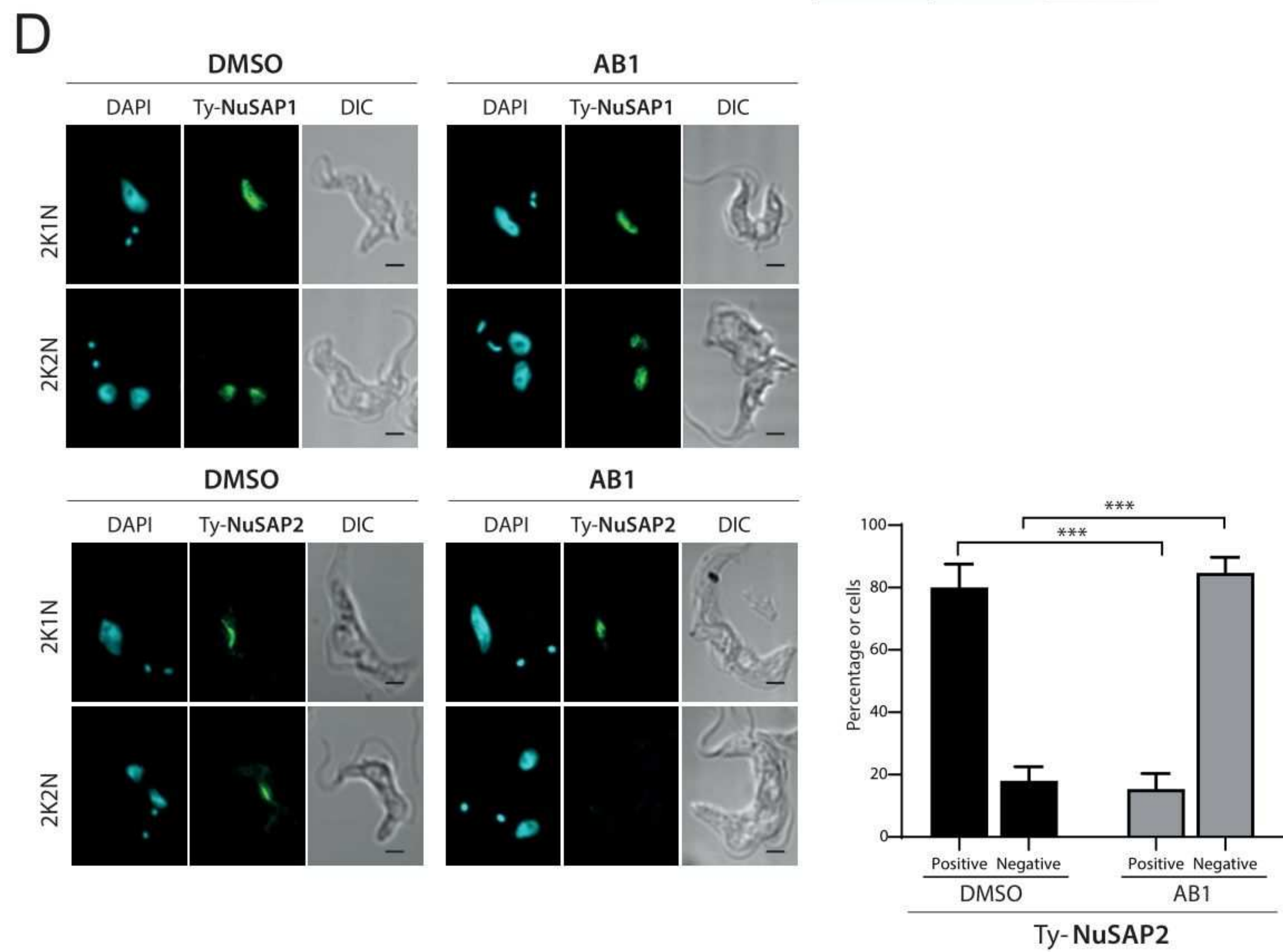
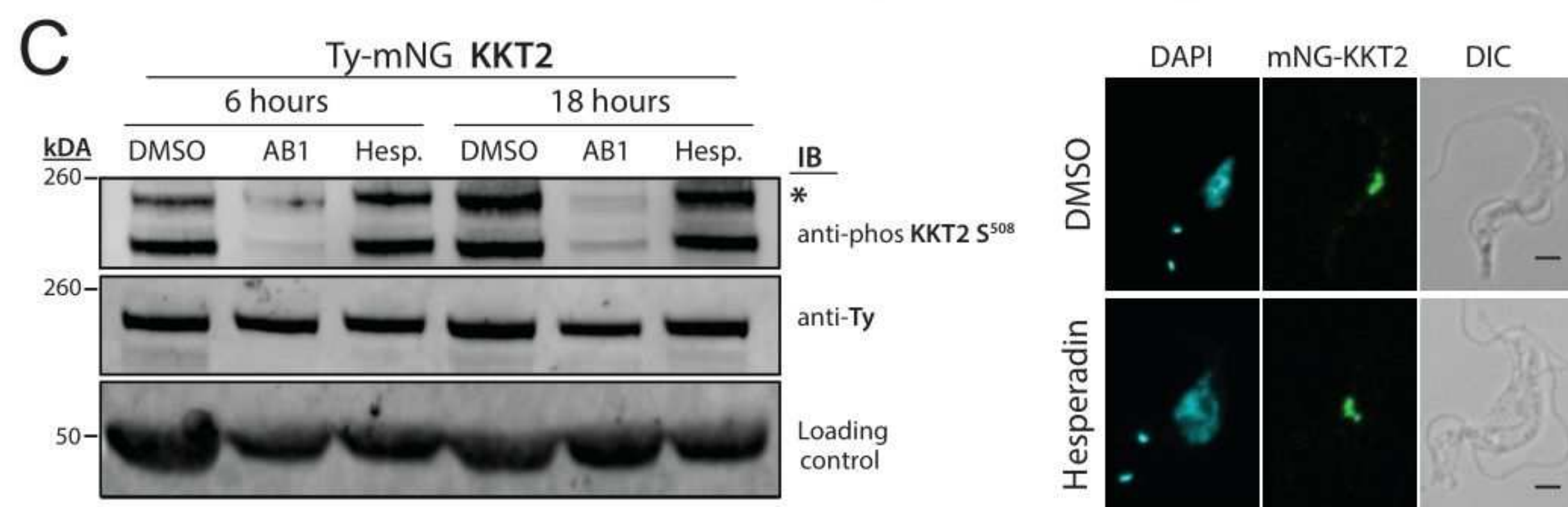
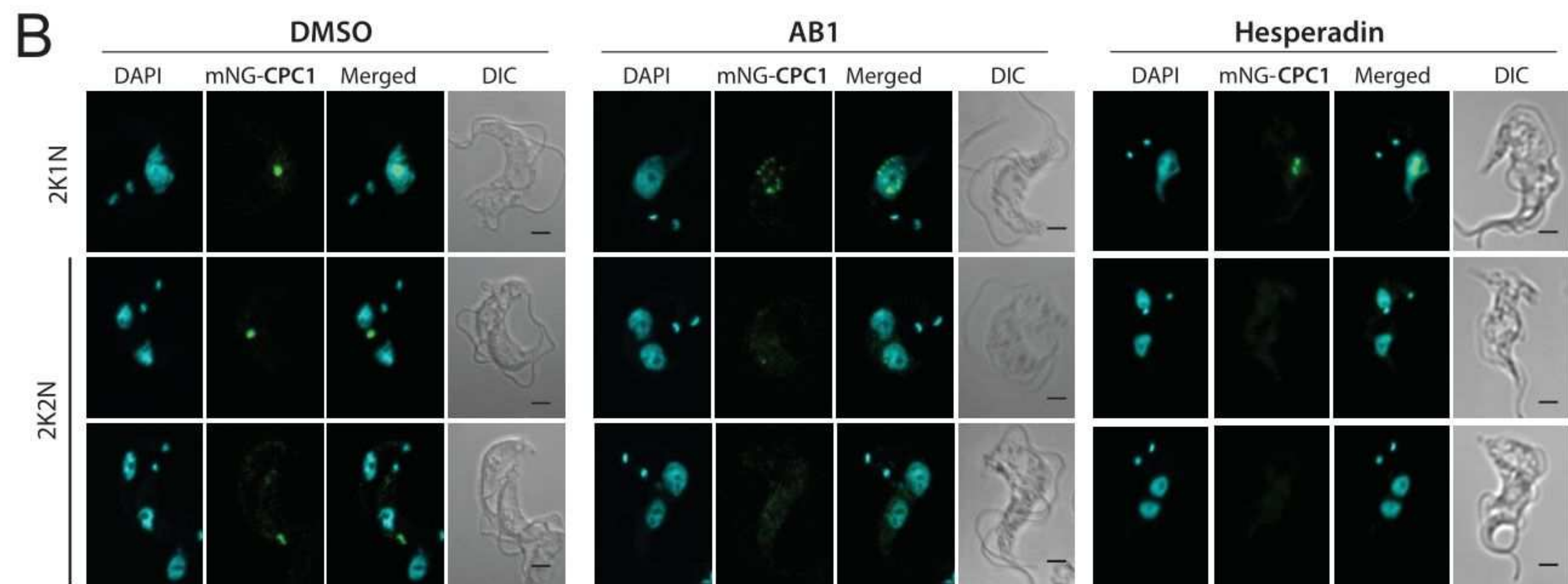
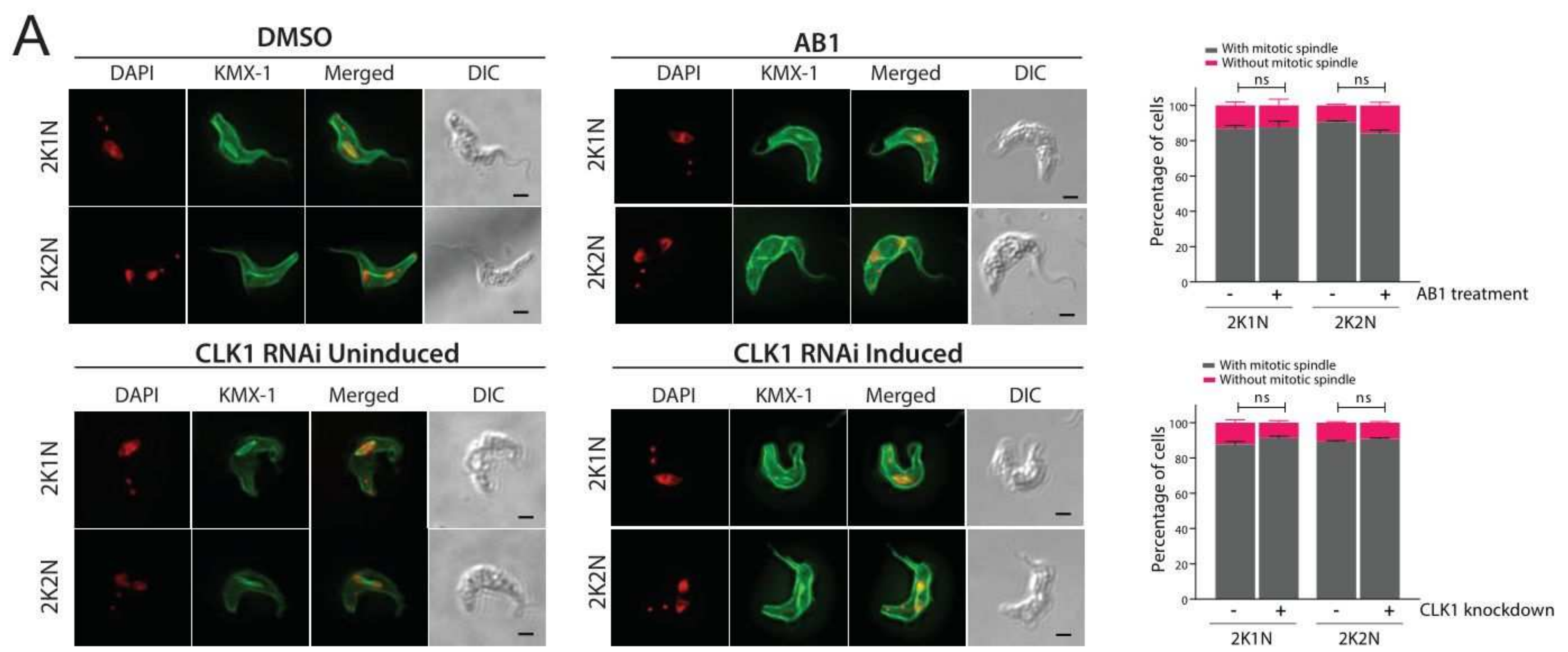
B



C

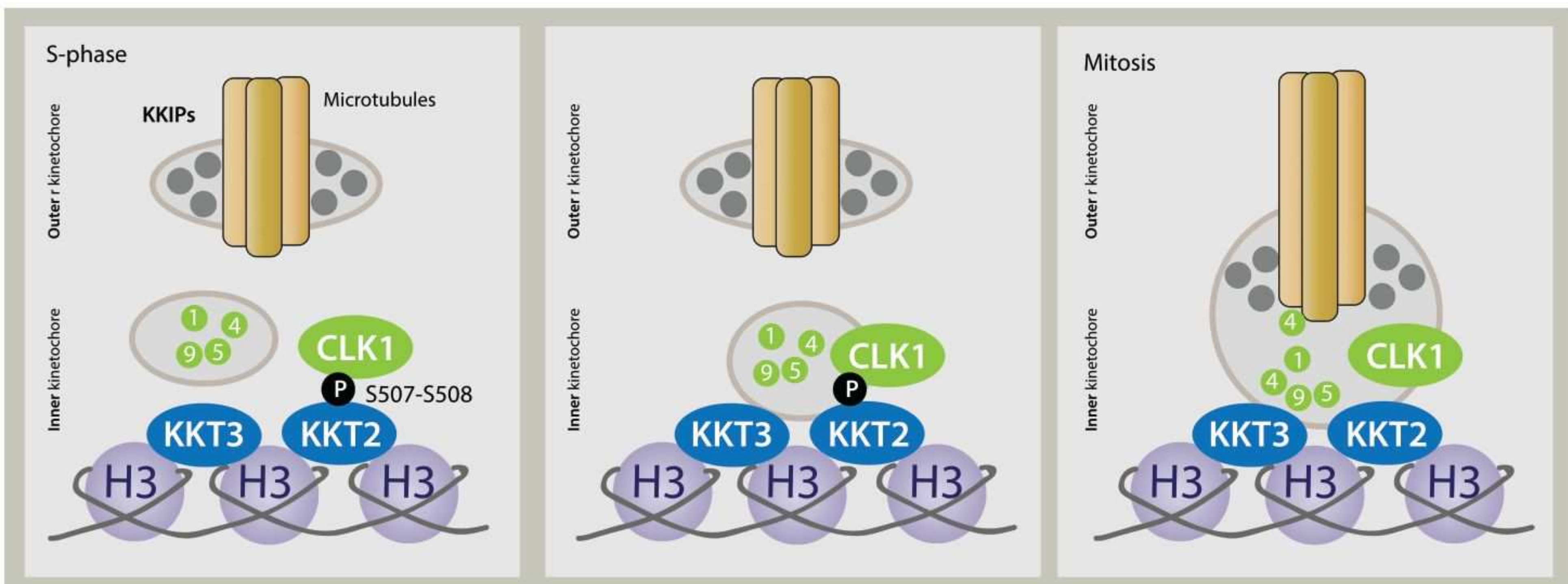




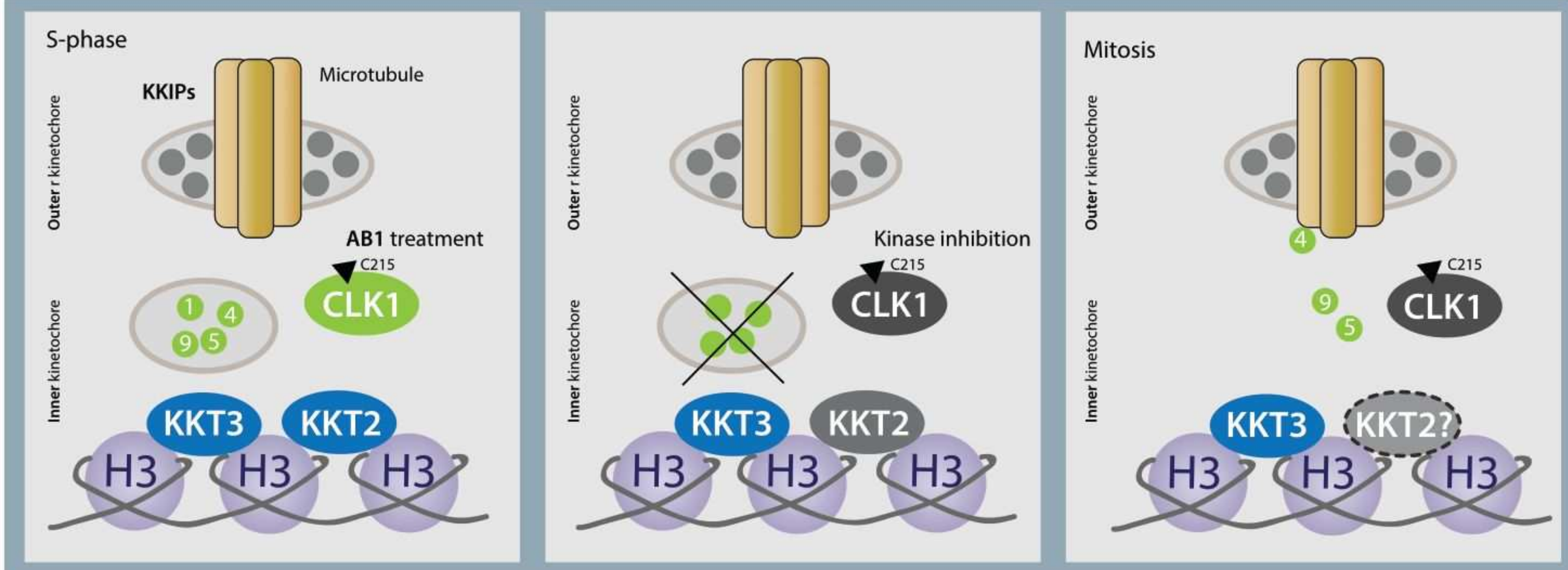




UNTREATED

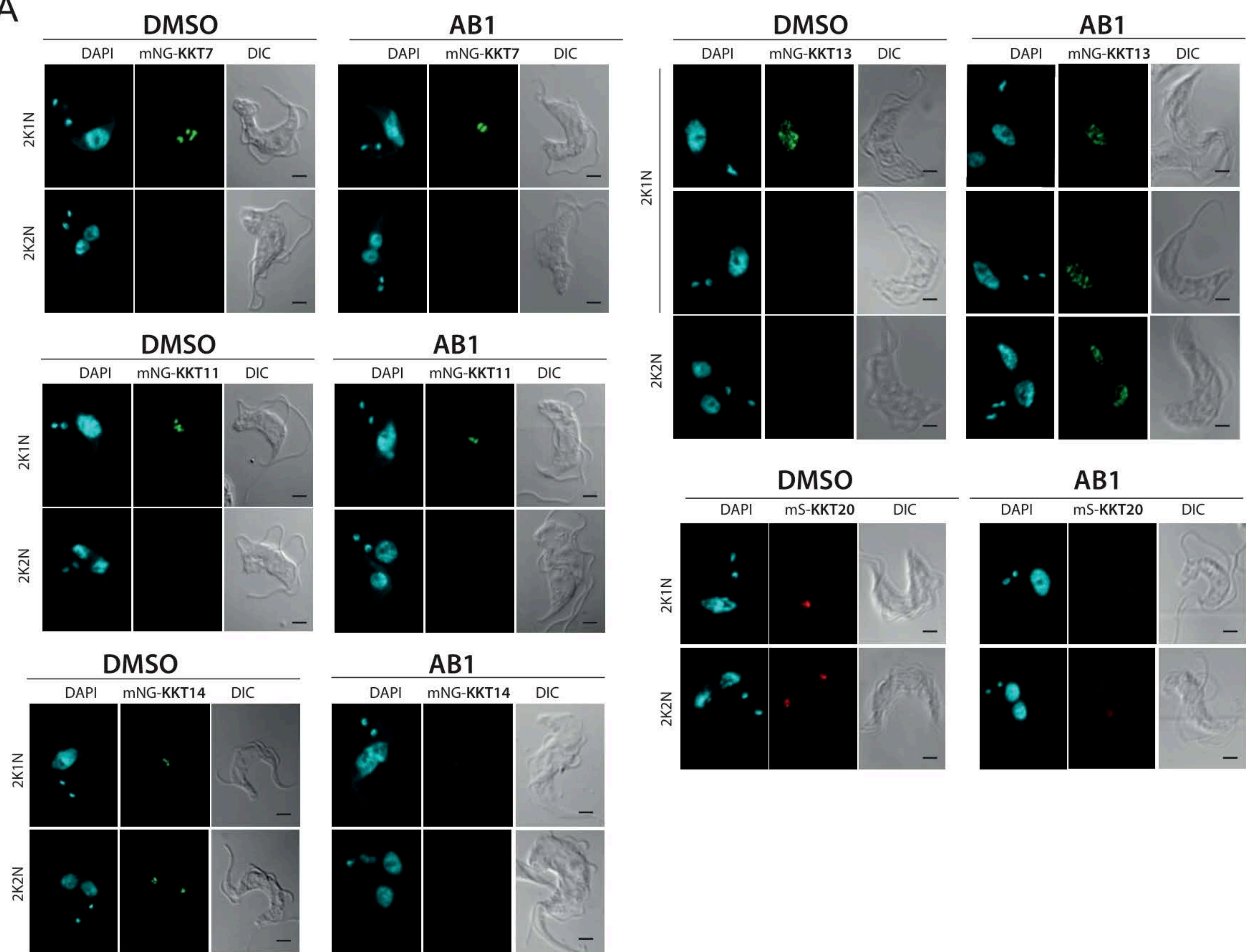


TREATED

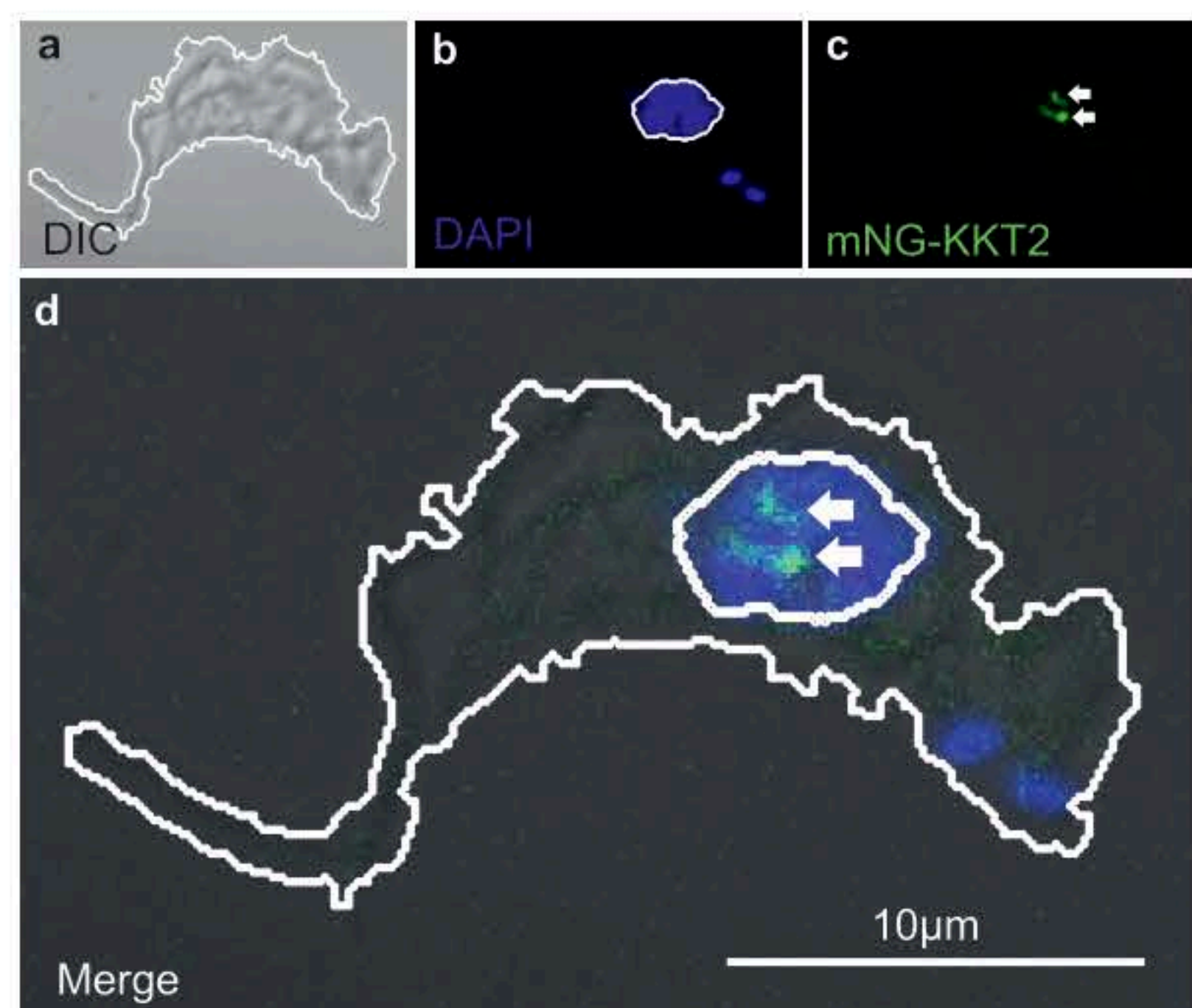




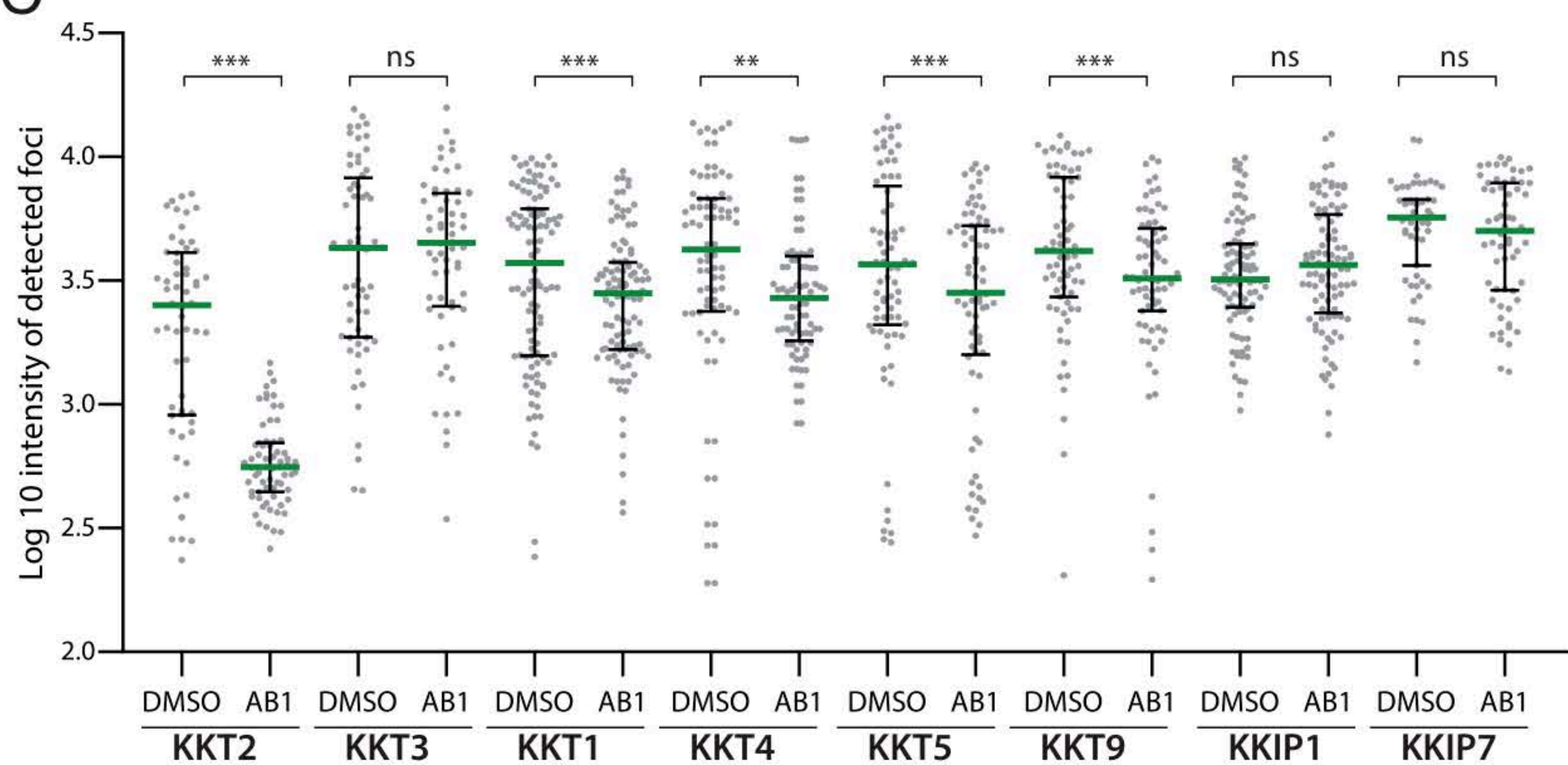
**A**



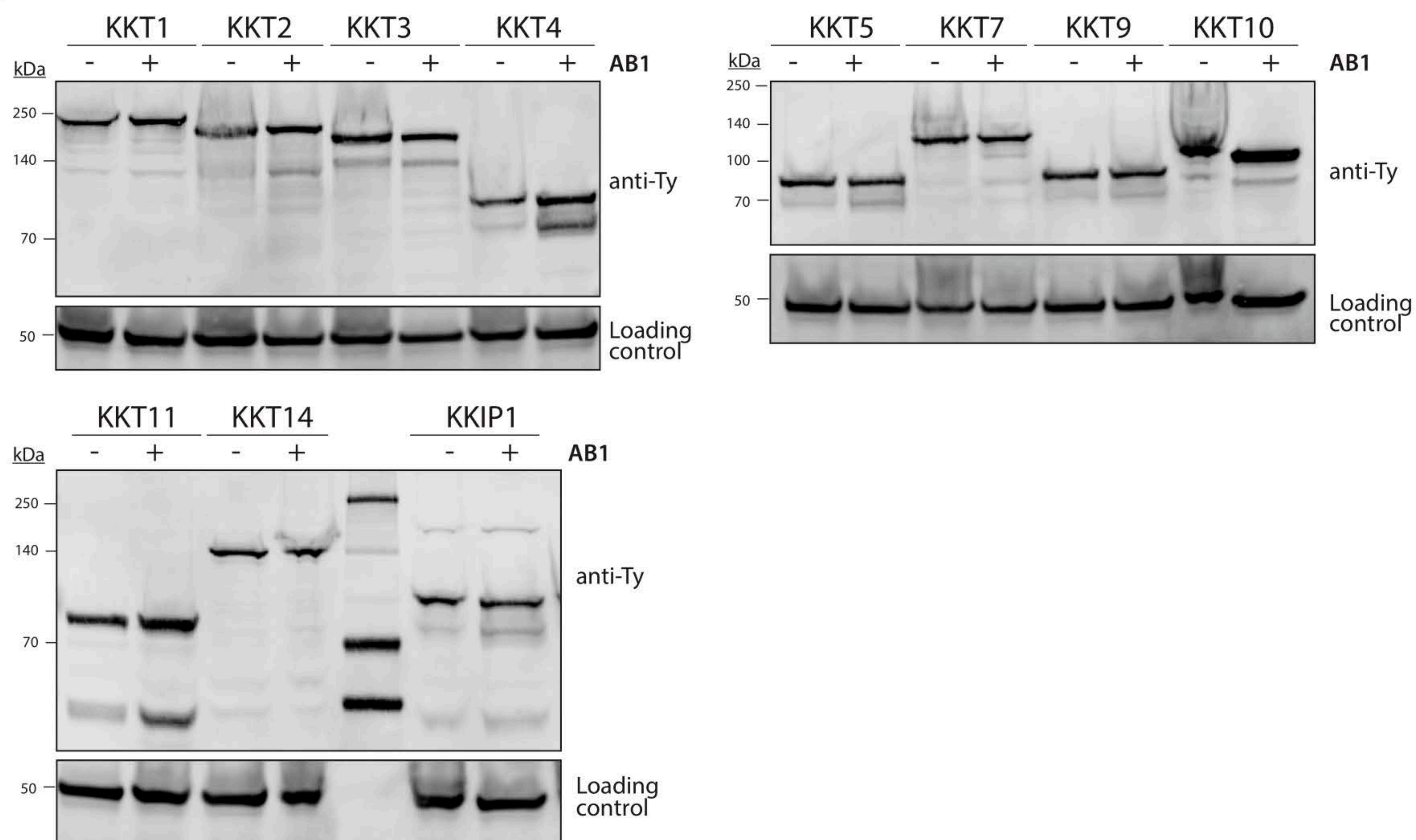
**B**



**C**

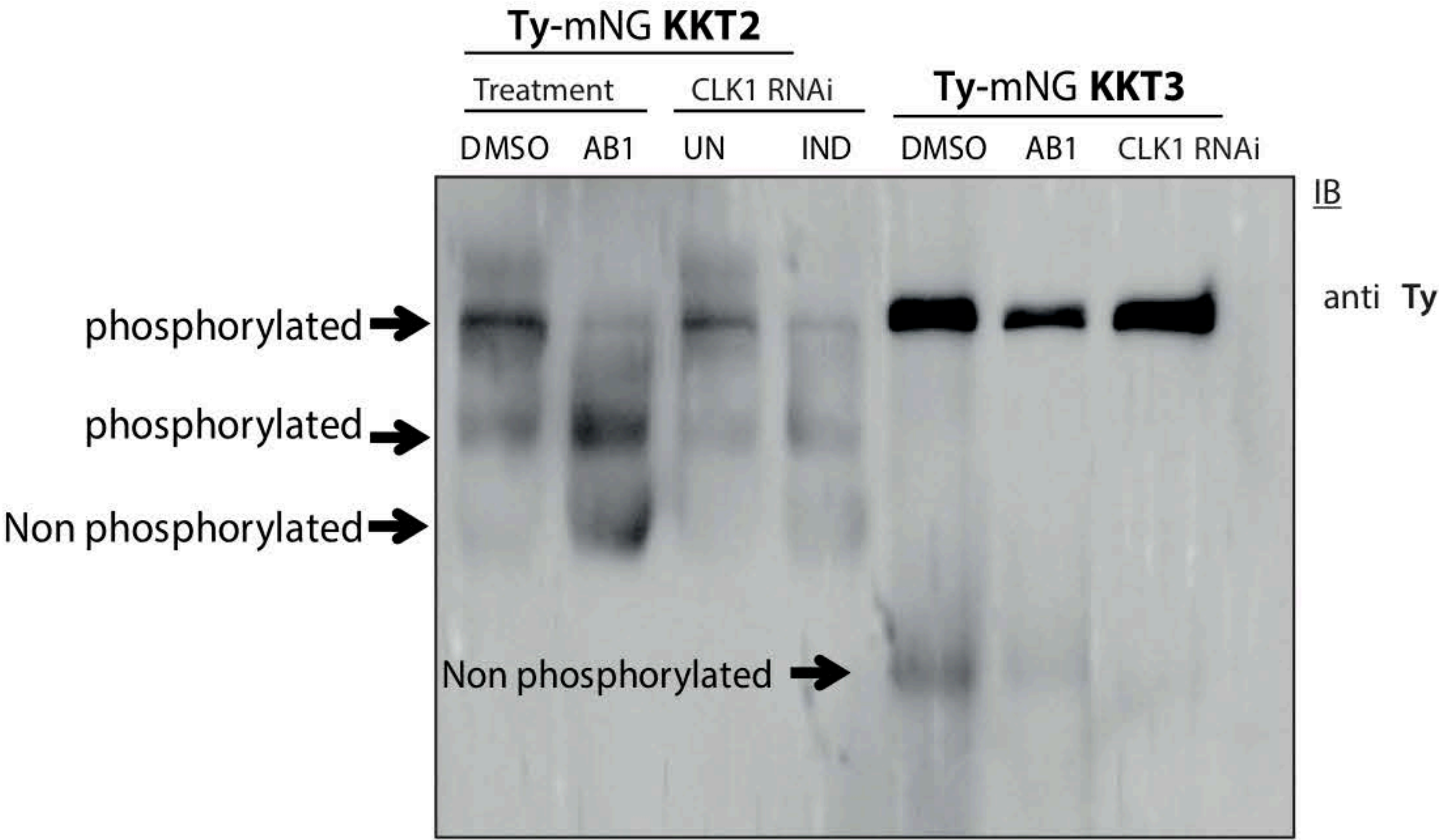


**D**

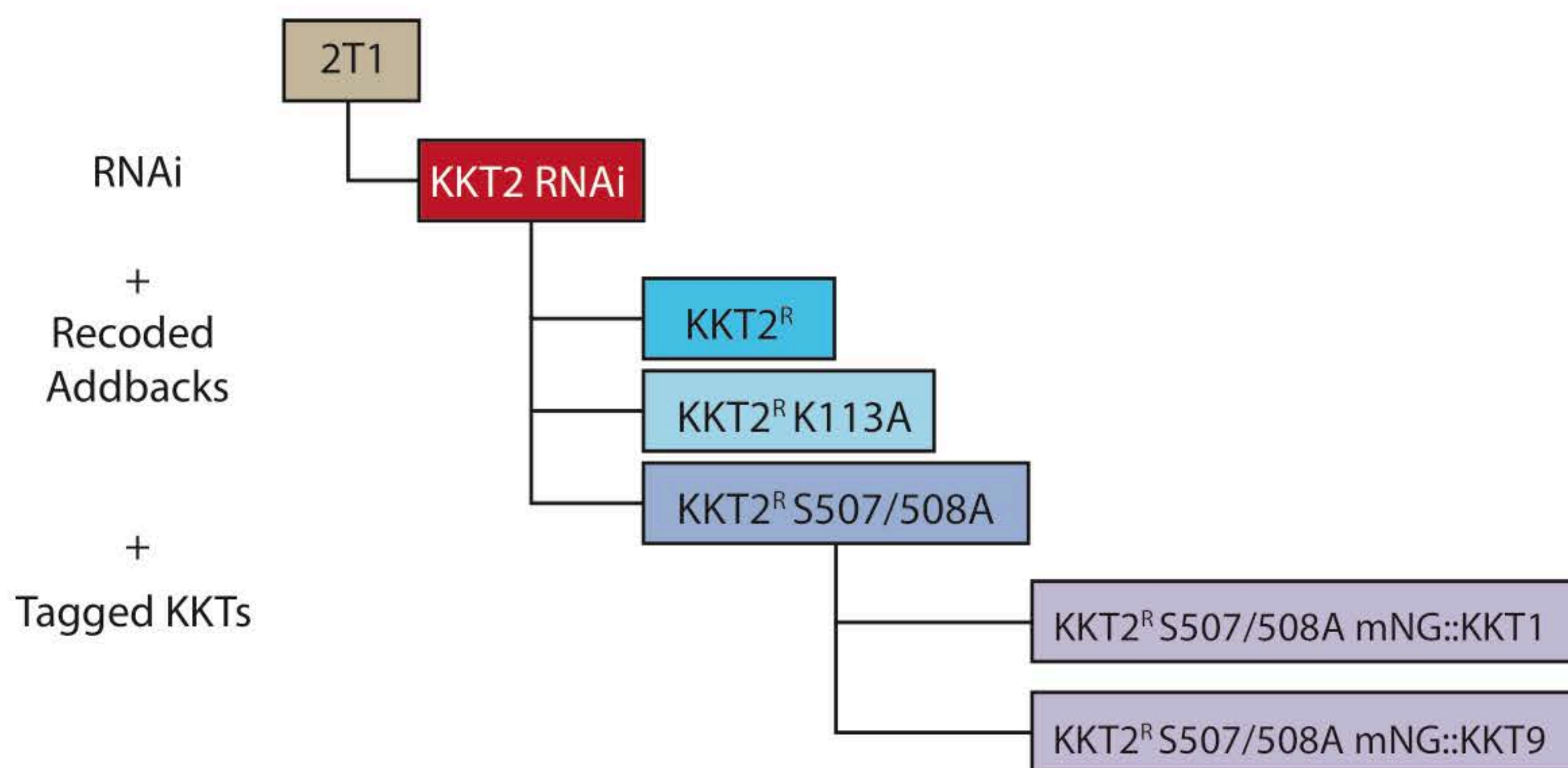
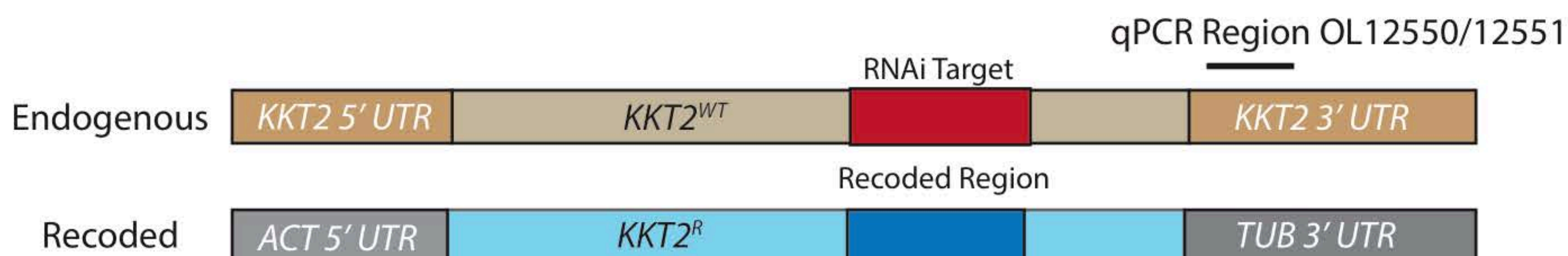
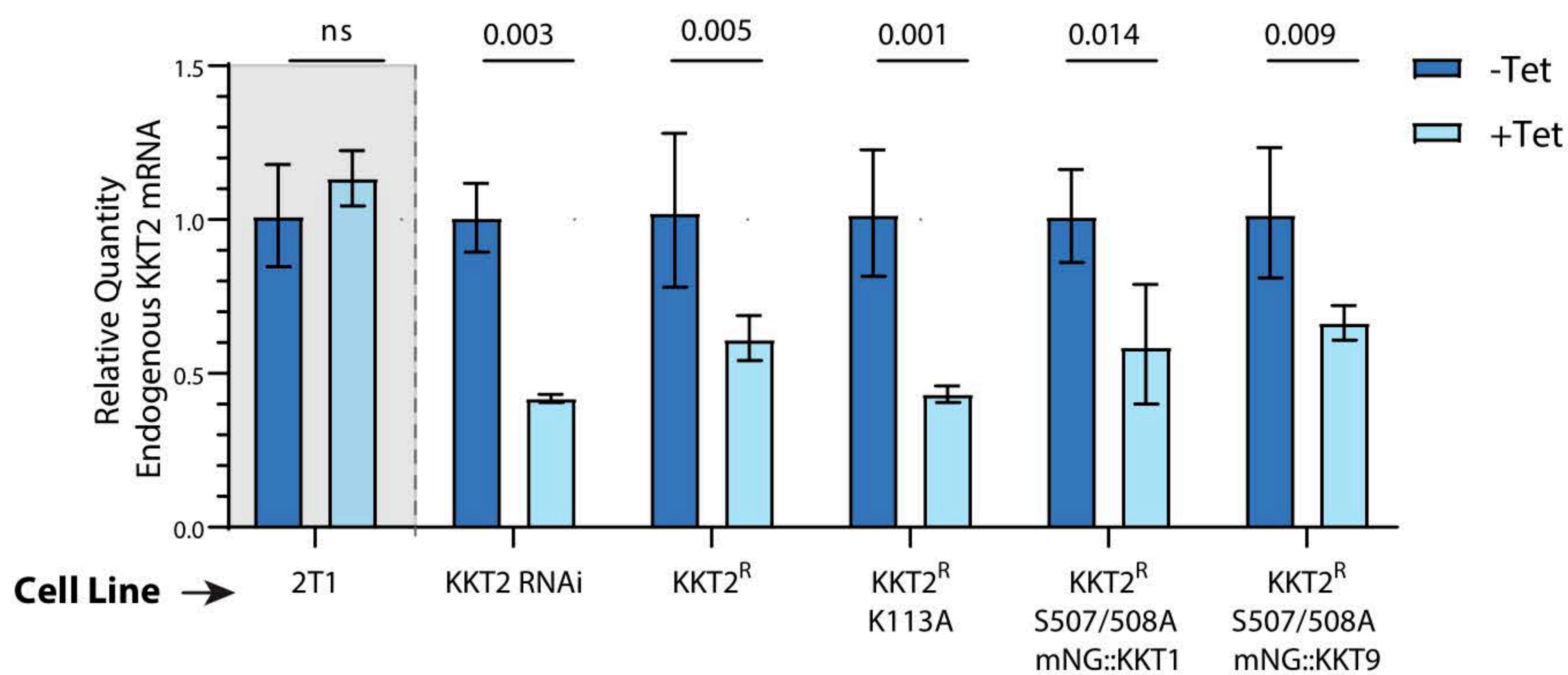
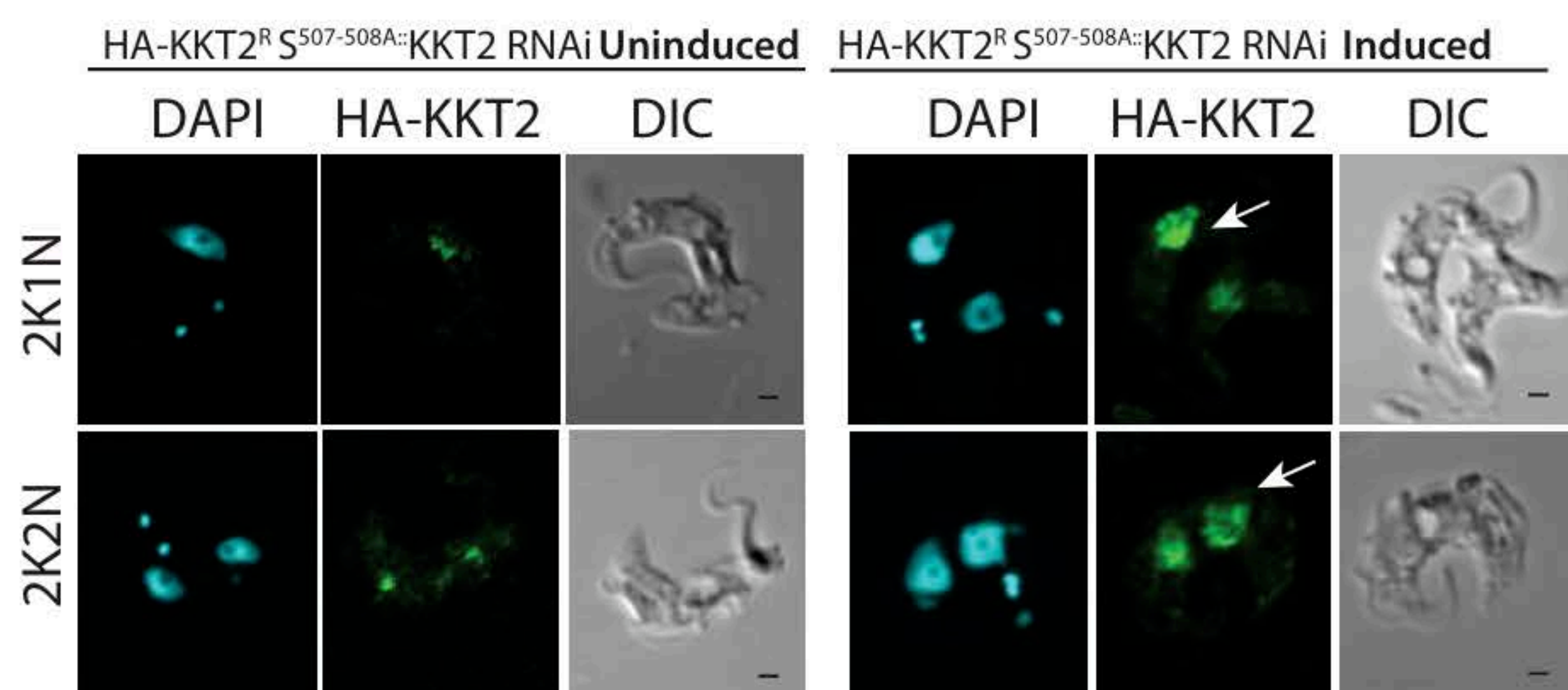
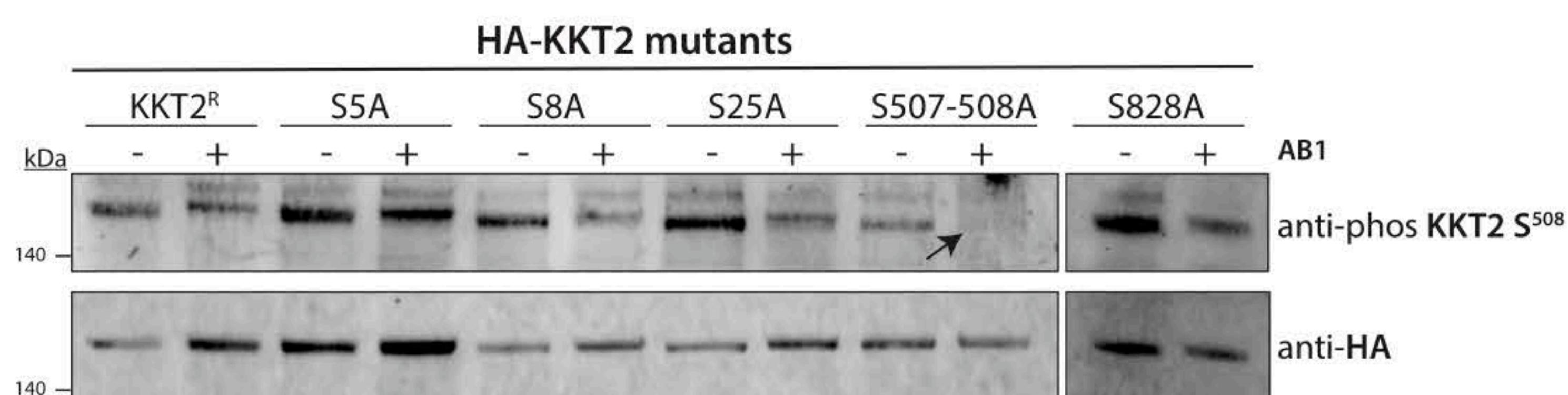




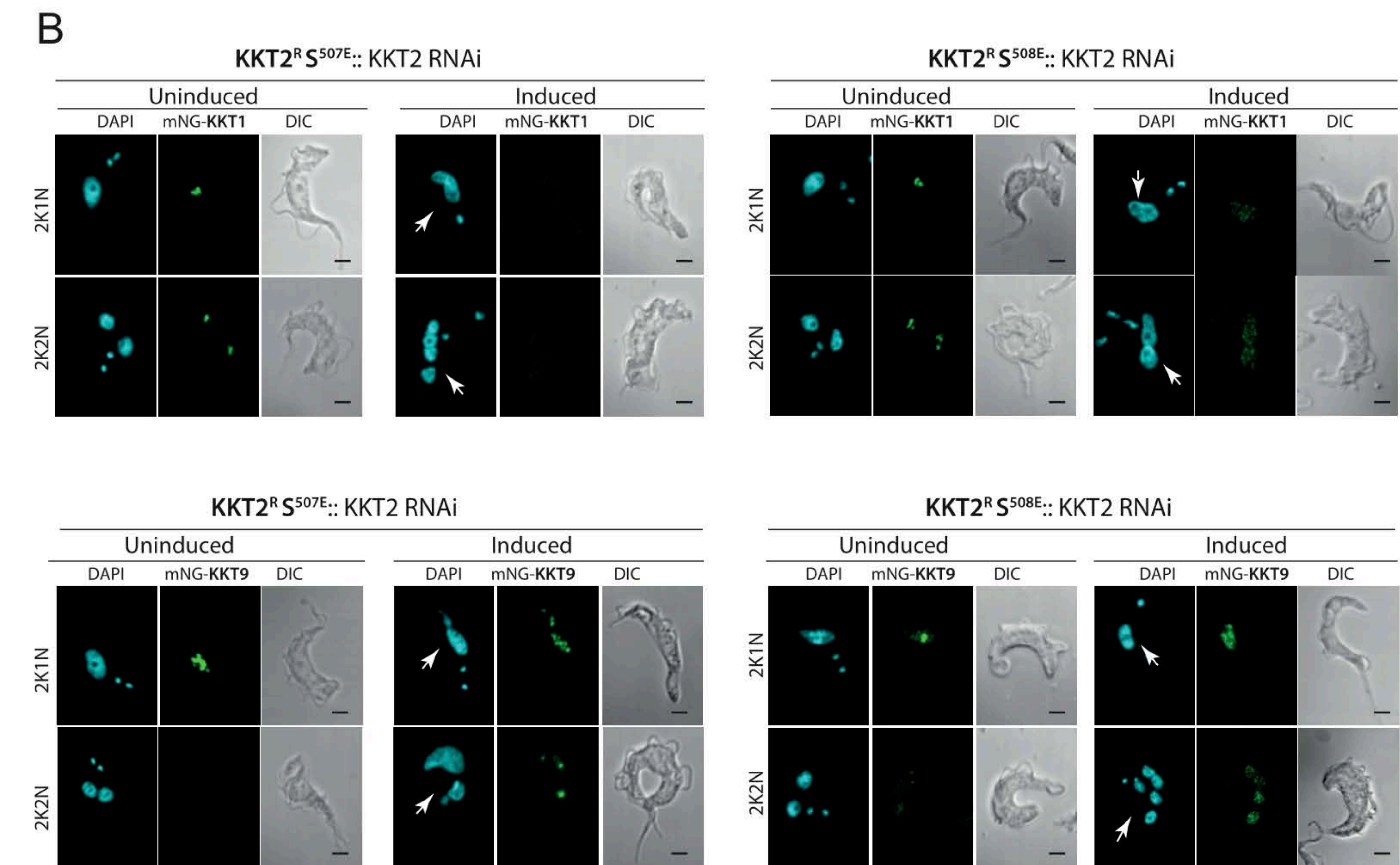
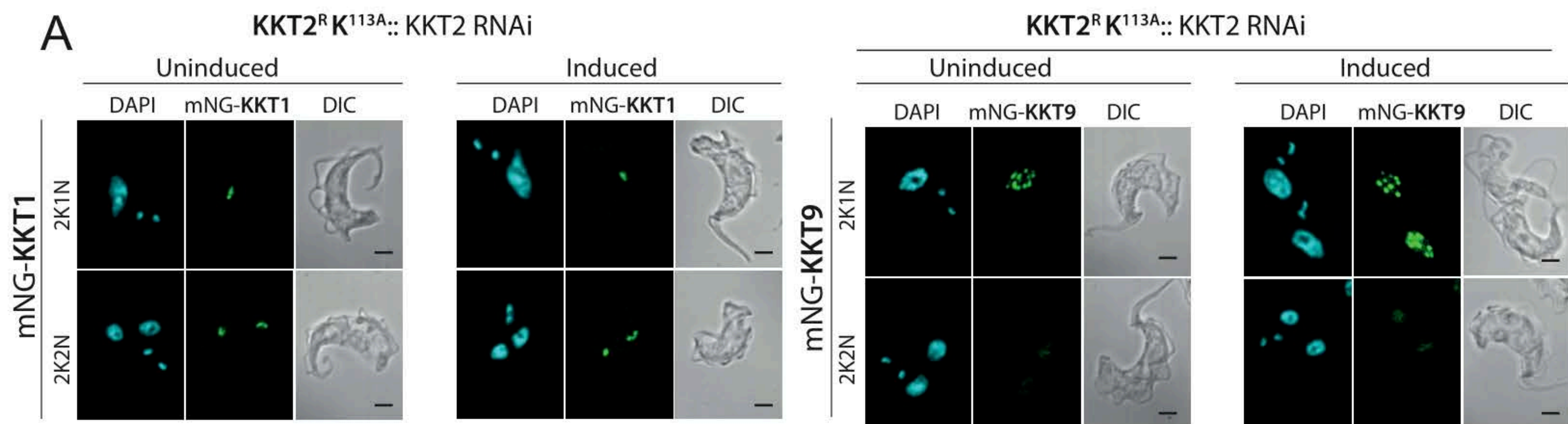
A

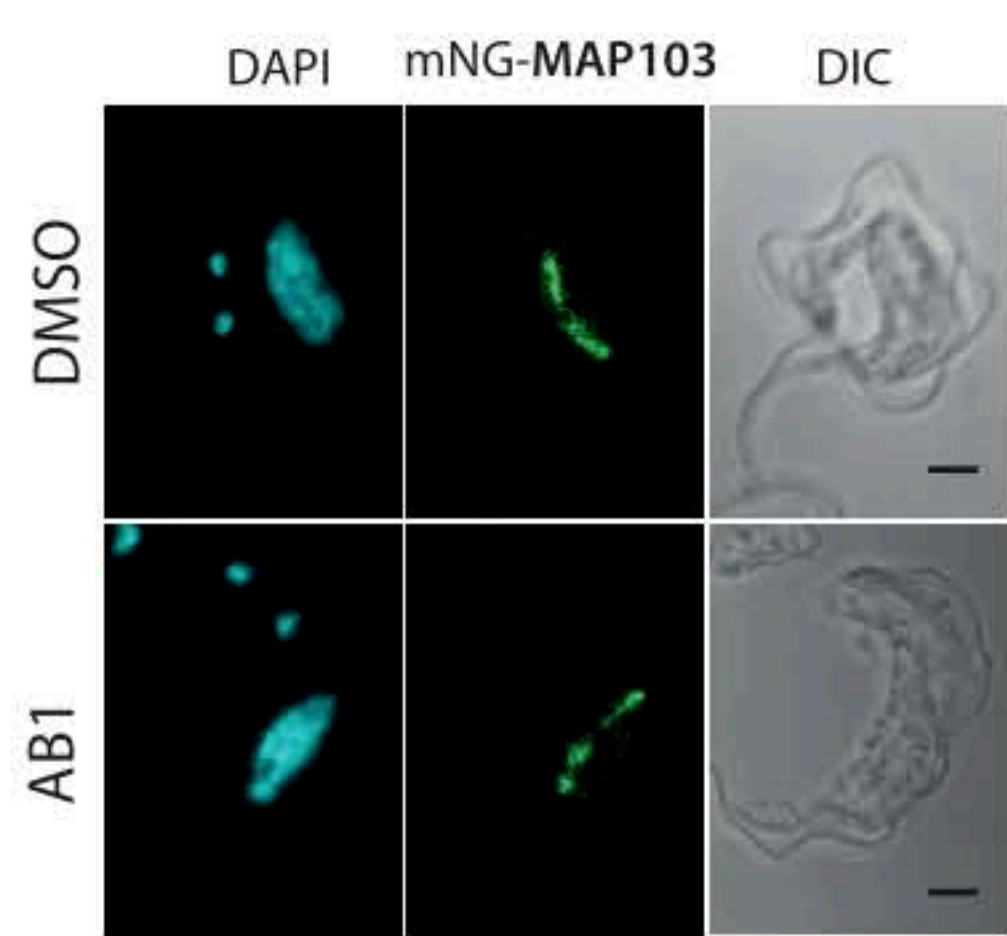
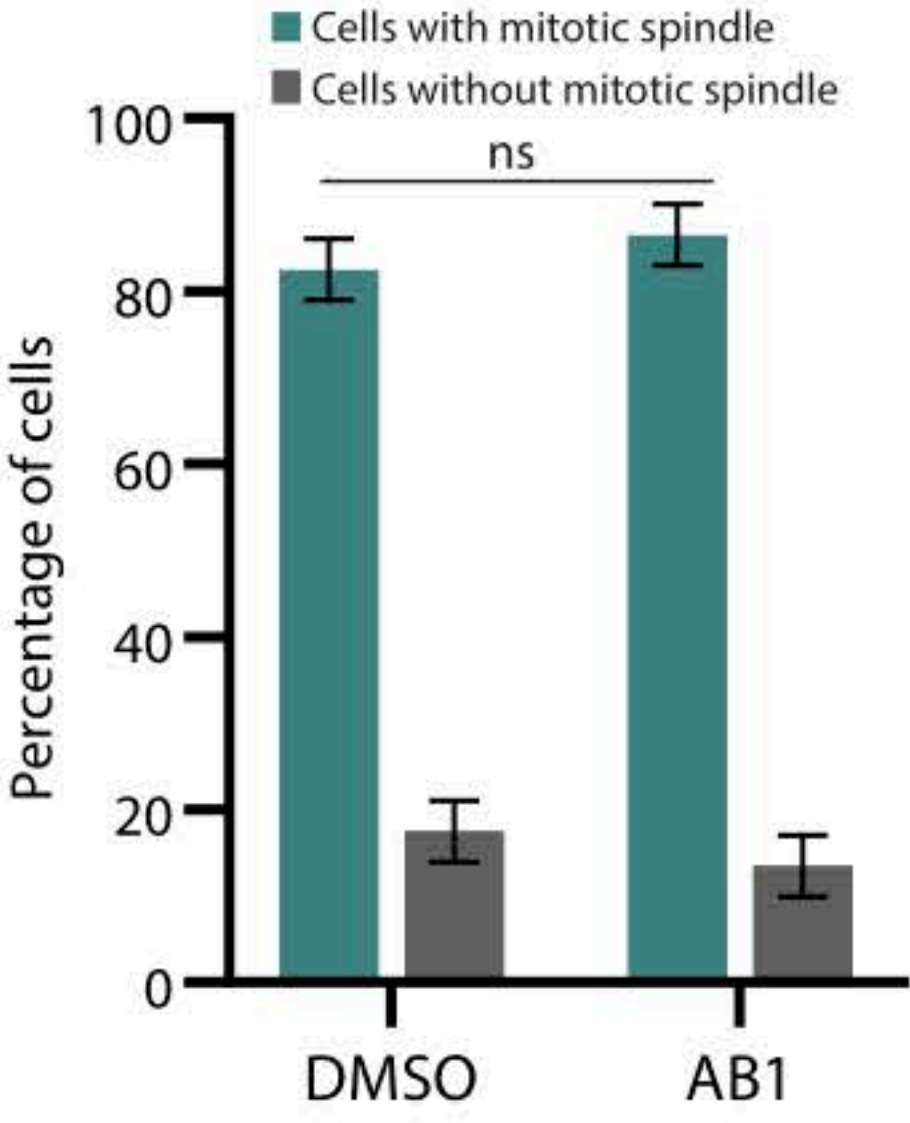




**A****B****C****D****E**









## Supplementary Methods

**Recoded Plasmids.** To express catalytically inactive KKT2 and phospho-mutants, the active site lysine (K113) and serine (S5, S8, S507-S508 and S828) were changed to alanine by mutating pGL2492, carrying the coding sequence for KKT2, using site directed mutagenic PCR as follows:

PRIMER SEQUENCES	MUTATION	PLASMID
5'- GTTCAATGTCGCGCCAGCGAGTC	KKT2 <sup>R</sup> S5A	pGL2795
3'- ATTCTAGATATTTTATGGCAGCAAC		
5'- CTCACCAGCGGCGCGTGACCGCG	KKT2 <sup>R</sup> S8A	pGL2796
3'- ACATTGAACATTCTAGATATTTTATGGCAG		
5'- CCCCCGCGGCGCGCTCTCCATGC	KKT2 <sup>R</sup> S25A	pGL2797
3'- CGCGGGGTGCGCTGACTC		
5'- AAGGGTCGGTGCAGCATTAAAGGCCGC	KKT2 <sup>R</sup> S507A-S508A	pGL2749
3'- GTTCCACGTTTGGGCTGTTTT		
5'- TAGACAGAATGCATGCGAGCCTTATGCACC	KKT2 <sup>R</sup> S828A	pGL2750
3'- GCTTCGGTTCTGACCCTC		
5'- GTGCGCCTTGGCAGTATCGTCGAAAC	KKT2 <sup>R</sup> K113A	pGL2850
3'- AACTCCCCGCCACTTGAC		
5'- AAGGGTCGGTGAATCATTAAAGGCCG	KKT2 <sup>R</sup> S507E	pGL2770
3'- GTTCCACGTTTGGGCTGT		
5'- GGTTCGGTTCCGAATTAAGGCCGC	KKT2 <sup>R</sup> S508E	pGL2759
3'- CTTGTTCCACGTTTGGGC		

## Antibodies

Antibody	Obtained from
Mouse Imprint Monoclonal <b>Anti-Ty1</b> antibody (clone BB2)	Sigma Aldrich
Mouse <b>Anti-HA</b> (clone 12CA5)	Roche
Mouse <b>Anti-EF1α</b> Antibody, (clone CBP-KK1)	Merck-Milipore
Rabbit <b>Anti-phospho KKT2 S<sup>508</sup></b>	Invitrogen
Mouse monoclonal anti- <b>KMX-1</b>	Keith Gull laboratory
StarBright™ Blue 520 Goat anti-Mouse IgG	BIORAD
StarBright™ Blue 700 Goat Anti-Mouse/Anti-Rabbit IgG	BIORAD

**RT-qPCR for validation of KKT2 RNA Knockdown.** RNAi inductions were set up to be able to collect  $2 \times 10^7$  trypanosomes at 24h post tetracycline addition. Total RNA was extracted from these cell pellets using the NEB Monarch RNA Miniprep kit to manufacturer's instructions. Contaminating gDNA was removed using TURBO DNA-free treatment (Invitrogen). One hundred nanograms of total RNA was then used to prime RT-qPCR reactions set up using Luna Universal One-Step RT-qPCR Kit (NEB), which were amplified and measured using the SYBR and ROX channels of an Applied Biosystems QuantStudio 3 System machine. Oligonucleotides were designed using Primer-BLAST against the 3' UTR of the KKT2 gene to allow quantification of the WT allele and avoid the RNAi stem-loop RNA and the recoded KKT2 allele's mRNA. Primer efficiencies were

previously verified to be between 95% and 105% using a standard curve analysis prior to relative quantitation experiments. Relative quantitation experiments were performed using the  $\Delta\Delta C_t$  method with the Tb927.10.12970 (C1) as an endogenous control (1). Samples for comparison were run in technical quadruplicates. No-reverse transcriptase and no-template controls were included on each plate for each sample condition, each in duplicate. Data were analysed in the RQ module of ThermoFisher Cloud to perform the relative quantitation including the T-test option for comparing induced to non-induced samples.

### KKT2 qPCR Primers

Oligo	Target	Gene ID	Sequence	Description	Efficiency
OL12565	<b>C1</b>	Tb927.10.12970	5'-TTGTGACGACGAGAGCAAAC	Endogenous control	100.14%
OL12566			3'-GAAGTGGTTGAACGCCAAAT		
OL12550	<b>KKT2</b> 3' UTR	Tb927.11.10520	5'-CGCTTCTGTGTTTCGGGTACT	KKT2	96.70%
OL12551			3'-AGGTGGTCGGACACTGGATA		

**Recombinant assays and enzyme purification.** Recombinant full-length CLK1 was produced as described (22). For KKT2 protein production, the KKT2 (aa 486 - 536) CDS was cloned in pET24-MBP-TEV vector, generating the plasmid NITD2500. Recombinant expression was carried out by lactose autoinduction in Terrific Broth containing 0.4% glycerol, 0.05% glucose, 0.05% lactose, 0.05% arabinose and buffered by 100 mM sodium phosphate (pH 7.0). In brief, 0.7 L of this media was inoculated at 0.1 OD600 with an overnight Luria Broth culture and shaken at 37 °C and 250 rpm for 2.5 hr. Then, temperature was lowered to 18 °C and the culture was allowed to grow and induced overnight and harvested 20-24 hr later. Cells are pelleted and stored at -80 °C prior to purification. Cell lysis was done by sonication in an ice bath (20 sec ON/OFF, 3 min active sonication at 70-110 watts power) in 40 mL Equilibration Buffer (25 mM HEPES pH 7.5 300 mM NaCl 5% glycerol 0.5 mM TCEP) and the clarified lysate is purified by IMAC on a 5 mL HisTrap column (GE Healthcare). The IMAC elution was further purified by sizing on a 300 mL Superdex 200 prep grade column (GE Healthcare) packed in a 2.6 cm diameter housing. Included volume fractions were pooled and analysed by SDS-PAGE or LC-MS.

To express recombinant KKT2<sup>S507-508A</sup>, plasmid NITD2500 was mutated using site directed mutagenic PCR as follows to give plasmid NITD2501:

PRIMER SEQUENCES	MUTATION	PLASMID
5'- GCGTGTGGGGgcagcaTTGCGCCCGC	KKT2 <b>S507-508A</b>	NITD2501
3'- GTCCCACGCTTAGGCTGT		

Recombinant CLK1 enzyme activity assays were performed in white 96 well, solid bottom plate (GREINER) by triplicate. The assay buffer contained 40 mM Tris (pH 7.5), 20 mM MgCl<sub>2</sub>, 0.1mg/ml BSA and 2 mM DTT. As indicated, kinase reaction contains the enzyme CLK1 (3 nM), and 1 micromolar or each indicated substrate. Maltose binding protein (MBP, Abcam ab219252) and DMSO were added as control of background or autophosphorylation respectively. ATP (10  $\mu$ M) was added to initiate the reaction. After 25 min reaction at room temperature, the ADP-Glo reagent and detection solution was added following the technical

manual of ADP-Glo™ kinase assay kit (Promega). The luminescence was measured on CLARIOstar BMG LABTECH microplate reader.

**Kinetochores foci intensity capture and analysis.** Cells were imaged using a Zeiss LSM 880 with Airyscan on an Axio Observer.Z1 inverted confocal microscope. A Plan-Apochromat 63x/1.4 oil objective lens was used to image 476 x 476 70nm pixels with a photomultiplier tube and 16x averaging at 38s/frame. DAPI and mNeonGreen excitation were from 405 and 488nm lasers with detection wavelengths 416-479nm and 491-589nm respectively. For measurement of kinetochores foci intensity, three channel image stacks of mNeonGreen labelled kinetochores components in fixed trypanosomes were analyzed using bespoke Matlab software (available here <https://github.com/awollman>). Blue, nuclear stained images were first segmented by thresholding using Otsu's method and applying a series of morphological transformations to remove holes and any objects smaller than 300-pixel area. This allowed the nucleus to be segmented and removed any detected mitochondria, also stained by DAPI. The whole cell was then segmented from the DIC image, using edge detection and similar morphological transformation, combined with watershedding, using the nuclear mask as 'seeds' for each cell. Finally, bright foci were detected in the mNeonGreen image using spot detection software optimized for detecting and characterizing low intensity foci in noisy cellular environments (2, 3). In brief, candidate foci were detected by thresholding and Gaussian masking, before their local background corrected intensity was determined and accepted if above a threshold based on the standard deviation of local pixel noise. Each detected cell was assigned a tracking number and foci categorized into each cell. This allowed for manual assignment into cell cycle stage. Fluorescent foci intensity was maintained in the linear range by optimizing the Imaging conditions using untreated cells to make the best use of the dynamic range of the detector while avoiding saturation. Microscope settings were kept constant between samples, and no saturation was detected, ensuring foci remained in the linear intensity regime.

**Recombinant assays and enzyme purification.** Recombinant full-length CLK1 was produced as described (4) For KKT2 protein production, the KKT2 (aa 486 - 536) CDS was cloned in pET24-MBP-TEV vector, generating the plasmid NITD2500. Recombinant expression was carried out by lactose autoinduction in Terrific Broth containing 0.4% glycerol, 0.05% glucose, 0.05% lactose, 0.05% arabinose and buffered by 100 mM sodium phosphate (pH 7.0). In brief, 0.7 L of this media was inoculated at 0.1 OD600 with an overnight Luria Broth culture and shaken at 37 °C and 250 rpm for 2.5 hr. Then, temperature was lowered to 18 °C and the culture was allowed to grow and induced overnight and harvested 20-24 hr later. Cells are pelleted and stored at -80 °C prior to purification. Cell lysis was done by sonication in an ice bath (20 sec ON/OFF, 3 min active sonication at 70-110 watts power) in 40 mL Equilibration Buffer (25 mM HEPES pH 7.5 300 mM NaCl 5% glycerol 0.5 mM TCEP) and the clarified lysate is purified by IMAC on a 5 mL HisTrap column (GE Healthcare). The IMAC elution was further purified by sizing on a 300 mL Superdex 200 prep grade column (GE Healthcare) packed in a 2.6 cm diameter housing. Included volume fractions were pooled and analysed by SDS-PAGE or LC-MS.

To express recombinant KKT2<sup>S507-508A</sup>, plasmid NITD2500 was mutated using site directed mutagenic PCR as follows to give plasmid NITD2501:

PRIMER SEQUENCES	MUTATION	PLASMID
------------------	----------	---------

5'- GCGTGTGGGGGgcagcaTTGCGCCCGC	KKT2 S507-508A	NITD2501
3'- GTCCCACGCTTAGGCTGT		

Recombinant CLK1 enzyme activity assays were performed in white 96 well, solid bottom plate (GREINER) by triplicate. The assay buffer contained 40 mM Tris (pH 7.5), 20 mM MgCl<sub>2</sub>, 0.1mg/ml BSA and 2 mM DTT. As indicated, kinase reaction contains the enzyme CLK1 (3 nM), and 1 micromolar or each indicated substrate. Maltose binding protein (MBP, Abcam ab219252) and DMSO were added as control of background or autophosphorylation respectively. ATP (10  $\mu$ M) was added to initiate the reaction. After 25 min reaction at room temperature, the ADP-Glo reagent and detection solution was added following the technical manual of ADP-Glo<sup>TM</sup> kinase assay kit (Promega). The luminescence was measured on CLARIOstar BMG LABTECH microplate reader.

1. S. Kabani et al., Genome-wide expression profiling of in vivo-derived bloodstream parasite stages and dynamic analysis of mRNA alterations during synchronous differentiation in *Trypanosoma brucei*. BMC Genomics. **10**, 427 (2009).
2. J. Wollman et al., Transcription factor clusters regulate genes in eukaryotic cells. Elife. **6** (2017), doi:10.7554/eLife.27451.
3. H. Miller, Z. Zhou, A. J. M. Wollman, M. C. Leake, Superresolution imaging of single DNA molecules using stochastic photoblinking of minor groove and intercalating dyes. Methods. **88**, 81–88 (2015).
4. M. Saldivia et al., Targeting the trypanosome kinetochore with CLK1 protein kinase inhibitors. Nat. Microbiol. **5**, 1207–1216 (2020).